Testplattform für GNSS Automotive

FKZ 50 NA 1205

TEGA

Abschlussbericht

TEGA-IFF- AP-3200-3500

Ausgabe 0

Revision 5

Autor:	Hans-Georg Büsing, Ulrich Haak IFF	Datum: 02.12.2013	
Projektleiter:	Günter Heinrichs, TEGA Project Leader		

Dokumenten-Information	
Projekt:	TEGA
Dokumenten-Titel:	Abschlussbericht
Dokumenten-Nr.:	TEGA-IFF- AP-3200-3500
Ausgabe/Revision:	0.1
Dateiname:	TEGA-IFF-Abschlussbericht_v06.doc
Umfang:	82

Copyright © 2013, TEGA Konsortium. Alle Rechte vorbehalten.

Änderungsnachweis

Ausgabe	Revision	Datum	Änderungen	Autor
0	1	29.10.2013	Ersterstellung, alle Kapitel	IFF
0	5	02.12.2013	Überarbeitung und Ergänzung	IFF

Copyright © 2013, TEGA Konsortium. Alle Rechte vorbehalten.

Inhaltsverzeichnis

Copyright © 2013, TEGA Konsortium. Alle Rechte vorbehalten.

Copyright © 2013, TEGA Konsortium. Alle Rechte vorbehalten.

Copyright © 2013, TEGA Konsortium. Alle Rechte vorbehalten.

Abbildungsverzeichnis

Copyright © 2013, TEGA Konsortium. Alle Rechte vorbehalten.

Tabellenverzeichnis

Copyright © 2013, TEGA Konsortium. Alle Rechte vorbehalten.

1. Einführung

1.1 Inhaltsangabe

Dieses Dokument dient als Abschlussbericht der vom IFF bearbeiteten Arbeitspakete 3200 und 3500 im Vorhaben TEGA. Es beinhaltet Zusammenfassungen der Aufgabenstellungen und Inhalte der Arbeitspakete.

1.2 Referenzdokumente

Tab. 1: TEGA Referenzdolumente

Ref.	Titel, Version	Autor	Revision / Datum
[R.1]	**Gesamtvorhabenbeschreibung**	IFEN	1.3 / 15.05.2012
[R.2]	**Zuwendungsbescheid**	DLR-RFM	- / 15.06.2012
[R.3]	**Vehicle Navigation Algorithms**	IFF	2.1 / 16.10.2012
[R.4]	**Test Report 'Fahrzeugdynamik'**	IFF	1.0 / 02.08.2013

1.3 Liste der Abkürzungen

Tab. 2: TEGA Abkürzungen

Acronym	Description
DLR	Deutsches Zentrum für Luft- und Raumfahrt e.V.
TEGA	Testplattform für GNSS Automotive
IFF	Institut für Flugführung, TU Braunschweig

Copyright © 2013, TEGA Konsortium. Alle Rechte vorbehalten.

2. Aufgabenstellung

Im Rahmen des Projektvorhabens ‚TEGA' sollten im Rahmen von drei Schwerpunkten eine Reihe von Kerntechnologien experimentell entwickelt werden, die Bestandteil zukünftiger Automobil-Testplattformen sein können.

Einer dieser Entwicklungsschwerpunkte bezieht sich auf experimentelle Erweiterungen des NavX®-NCS Multi-GNSS-Konstellationssimulators der IFEN GmbH, die als experimentelle Prototypen realisiert und deren Leistungsfähigkeit dann verifiziert werden soll.

Die primäre Zielsetzung der vom IFF bearbeiteten und hier dokumentierten Teilarbeitspakete innerhalb dieses Entwicklungsschwerpunkts ist die experimentelle Entwicklung einer realistischen Fahrdynamik-Simulation auf Basis des NavX®-NCS GNSS Simulators.

Dazu sollen zusätzlich zu den Satellitensignalen Messdaten erzeugt werden, die üblicherweise aus Fahrzeugen über die CAN Schnittstelle gesendet werden. Ausgangspunkt ist die dabei Trajektorie, die als Grundlage zur GNSS-Signalgenerierung durch den Konstellationssimulator dient. Aus dieser Trajektorie wird durch geeignete Aufbereitung der Zustandsvektor eines Rereferenzpunktes am Fahrzeug berechnet.

Darauf aufbauend soll durch eine Invertierung eines geeigneten Fahrzeugkinematikmodells die Punktbewegung auf die räumliche Ausdehnung des Fahrzeuges erweitert werden. So können idealisierte Rohdaten der Fahrzeugsensoren abgeleitet werden.

Basierend auf der so erzeugten Trajektorie sowie der Zustände an den relevanten geometrischen Punkten des Fahrzeuges sollen charakteristische Fehlereinflüsse der entsprechenden Sensoren emuliert werden. Typische Messfehler, mit denen derzeitige Seriensensorik typischerweise behaftet ist, sind beispielsweise Nullpunkt- und Skalenfaktorfehler, Einfluss von Einbaufehlern des Sensors, Vibration des Sensorträgers oder das Messrauschen des Sensors. Zum Abschluss erfolgt eine Diskretisierung der Sensorwerte, um die, der digitalen Datenübertragung geschuldete, begrenzte Auflösung der Messwerte nachzuahmen.

2.1 Planung und Ablauf

Die Bearbeitung der Aufgabenstellung war in zwei Arbeitspakte (AP 3200 und AP 3500) unterteilt. Das erste Arbeitspaket umfasste im Wesentlichen die theoretische Herleitung und Validierung der relevanten Algorithmen. Die experimentelle Validierung wurde im zweiten Arbeitspaket durchgeführt.

AP 3200 startete mit Projektbeginn und hatte einen Umfang von 8 MM Es wurde plangemäß mit der Abgabe der technischen Note (TN) 5 abgeschlossen.

Die Bearbeitung von Arbeitspaket 3500 begann sechs Monate nach Projektbeginn und belief sich auf einen Umfang von 11 MM. Ergebnis dieses Arbeitspakets ist das Dokument TN 6.

Copyright © 2013, TEGA Konsortium. Alle Rechte vorbehalten.

2.2 Wissenschaftlicher und technischer Startpunkt

Im Rahmen der Forschung am Institut für Flugführung ist ein modularer Softwarebaukasten in ADTF (Automotive Data and Time Triggered Framework) entstanden. Dieser beinhaltet zum einen die Anbindung von GNSS Empfängern, Fahrzeugsensorik und Korrekturdaten sowie Tools zur Auswertung und Visualisierung. Weiterhin ist in dieser Entwicklungsumgebung eine Ortungslösung implementiert, die auf Basis der genannten Daten den gegenwärtigen Fahrzeugzustand errechnet. Zu den verwendeten Fahrzeugsensorendaten gehören die Radgeschwindigkeiten, die Gierrate sowie die Informationen über die Längsbeschleunigung. Mit Hilfe dieser Evaluationsumgebung kann die Funktionsfähigkeit der Testplattform validiert und mit realen im Fahrversuch gewonnen Daten verglichen werden.

2.3 Zusammenarbeit mit anderen Stellen

Eine Zusammenarbeit mit anderen Stellen war im Rahmen der beiden durchgeführten Arbeitspakte nicht vorgesehen.

Copyright © 2013, TEGA Konsortium. Alle Rechte vorbehalten.

3. Erzielte Ergebnisse

Im Rahmen des TEGA-Projekts wurden für die vom IFF bearbeiteten Arbeitspakte zwei Zwischenberichte angefertigt, welche die geleistete Arbeit und die erzielten Ergebnisse dokumentieren.

Arbeitspaket 3200 umfasste die Erstellung eines Algorithmendokumentes „Fahrzeugnavigation“. Der in diesem Rahmen erstellte erste Zwischenbericht [R.3] vom 16.10.2012 beinhaltet die Herleitung der Algorithmen zur Simulation von Fahrzeugsensordaten unter Berücksichtigung der Kinematik von Straßenfahrzeugen und ist in Anhang A zu finden.

Das zweite Arbeitspaket (AP 3500) diente der experimentellen Validierung des Systems in der Evaluationsumgebung des IFF. Der zum Abschluss des Arbeitspakets erstellte Zwischenbericht dokumentiert die Ergebnisse und ist in Anhang B zu finden. Die in diesem Abschnitt gezeigten Ergebnisse stellen eine kurze Zusammenfassung des Berichts dar.

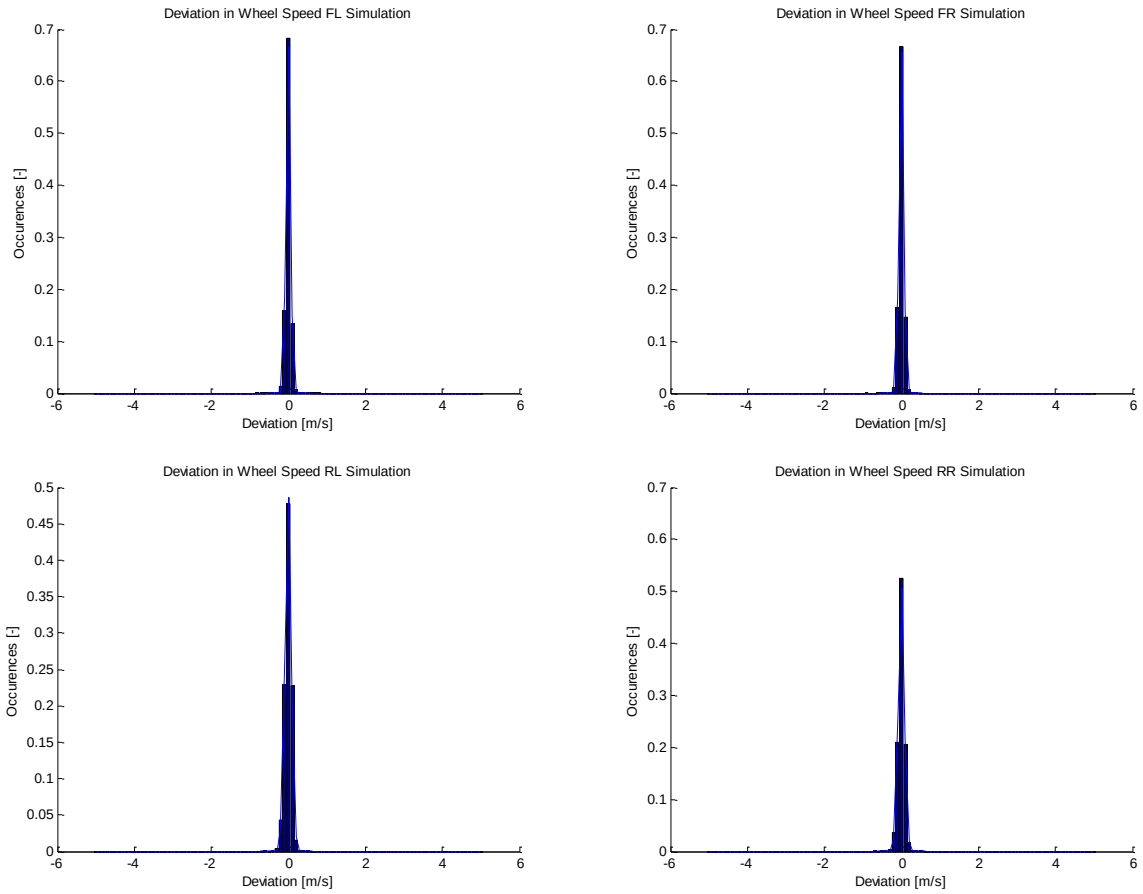

Abb. 1: Fehlerhistogramm der Radgeschwindigkeiten in einem Autobahnszenario

Die durchgeführte Validierung basiert auf dem Vergleich gemessener und emulierter Daten. Die gemessenen Daten wurden mit einem VW Passat, der dem IFF als Versuchsträger dient,

Copyright © 2013, TEGA Konsortium. Alle Rechte vorbehalten.

unter verschiedenen Umgebungsszenarien aufgezeichnet. Der im Passat verwendete GNSS-Empfänger diente dabei der Generierung einer Referenztrajektorie.

Unter Verwendung dieser Trajektorie konnten simulierte Messdaten für die Raddrehzahlsensoren erzeugt werden, deren Vergleich mit den aufgezeichneten ‚realen' Messdaten die Gültigkeit des verwendeten Modells nachweist.

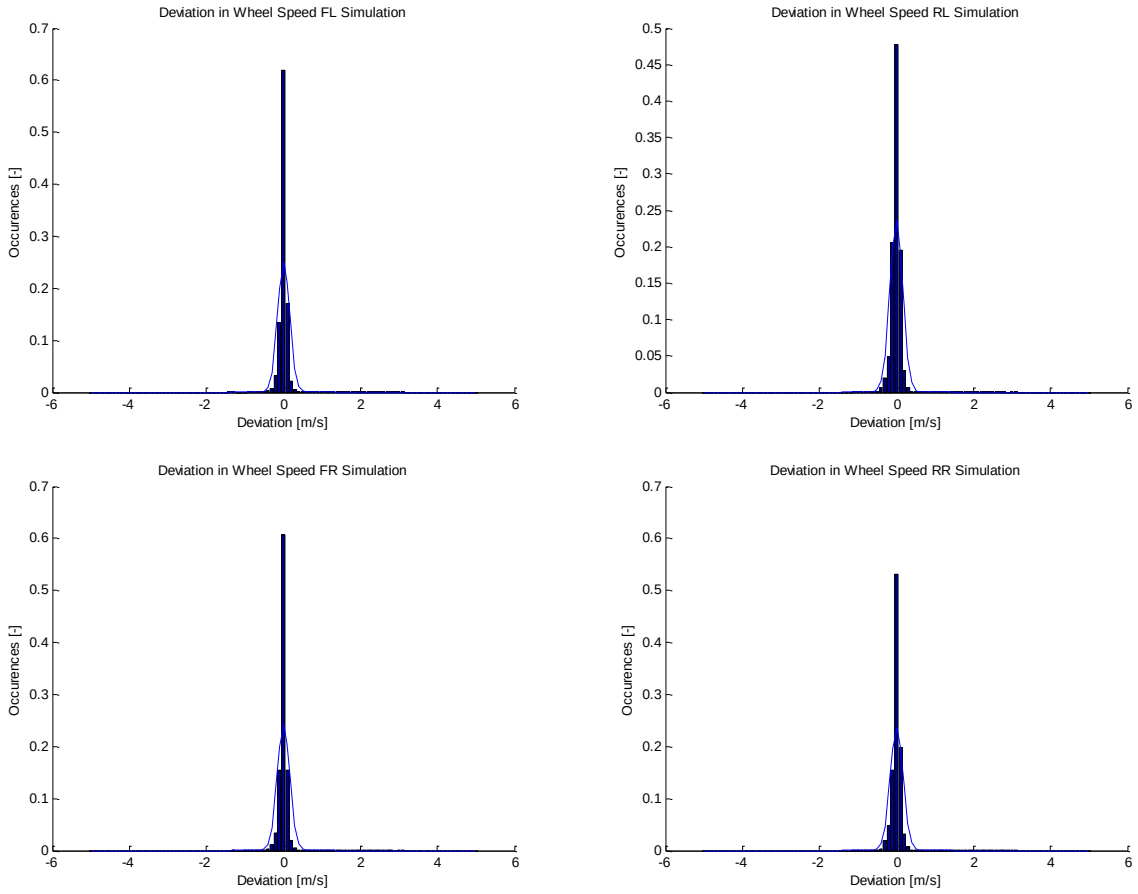

Abb. 2: Fehlerhistogramm der Radgeschwindigkeiten in einem kombinierten Autobahn-/Landstraßen-/Stadtszenario

Dabei wurde davon ausgegangen, dass ein mittelwertfreier, gaußverteilter Restfehler zwischen Modell und Messwerten systematische Fehler des Modells ausschließt. Die Abbildungen Abb. 1, Abb. 2 und Abb. 3 zeigen, dass der Restfehler diese Anforderung erfüllt. Zudem ist die Fehlerverteilung in erster Näherung szenarienunabhängig und weist außerdem eine sehr geringe Standardabweichung im unteren Dezimeterbereich auf.

Copyright © 2013, TEGA Konsortium. Alle Rechte vorbehalten.

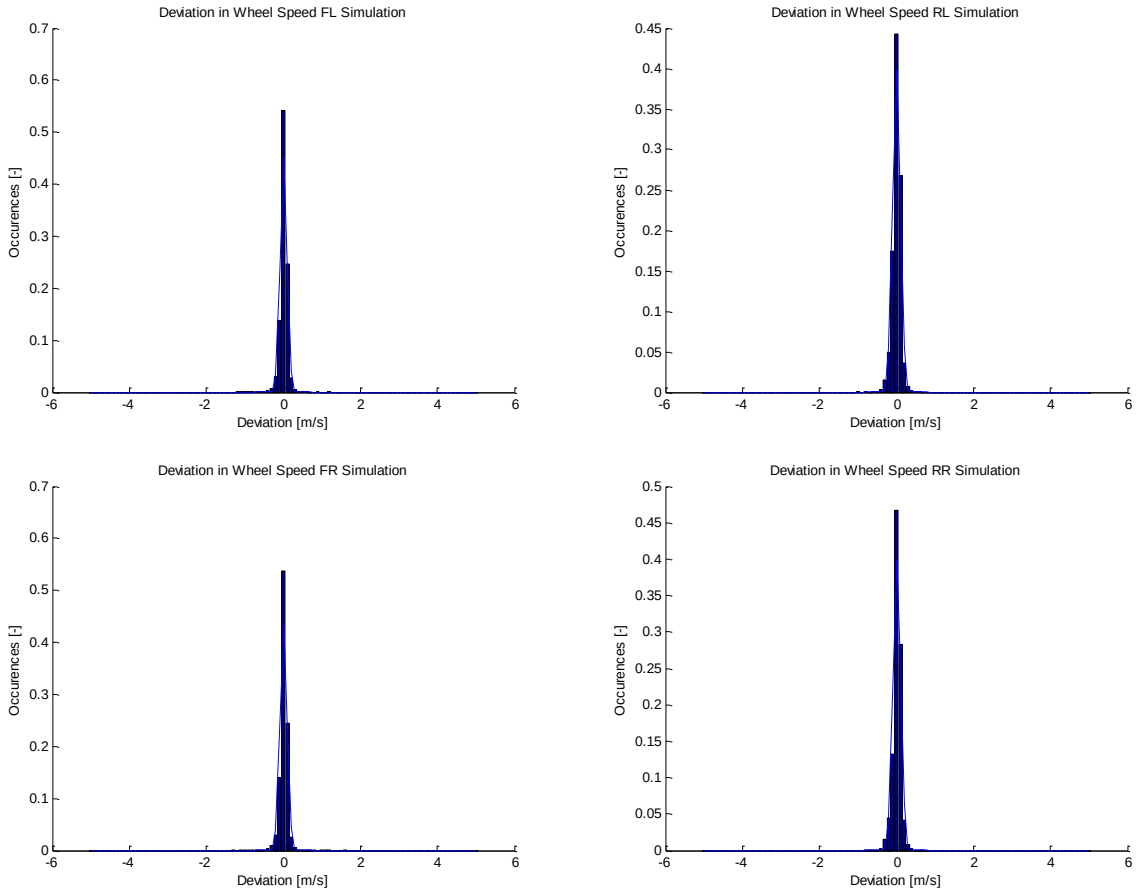

Abb. 3: Fehlerhistogramm der Radgeschwindigkeiten in einem städtischen Szenario

Durch die Auswertung der durchgeführten Versuche konnte experimentell nachgewiesen werden, dass die im Rahmen des Arbeitspakets 3200 hergeleiteten Algorithmen zur Modellierung fahrzeugtypischer Sensoren für die gestellte Anforderungen gültig sind. Für einen detaillierten Einblick in die Auswertung sei auf Anhang B verwiesen.

Des Weiteren sind in Anhang C Matlab-Skripte zu finden, mit denen die Aufbereitung der Trajektorien durchgeführt wurde.

Copyright © 2013, TEGA Konsortium. Alle Rechte vorbehalten.

4. Weitere Darstellungen

Auf weitere Darstellungen bezüglich Finanz- oder Verwendungsnachweise sei auf die jährlichen Zwischennachweise und die nichttechnischen Kurzberichte verwiesen.

4.1 Positionen des zahlenmäßigen Nachweises

Der Zahlenmäße Nachweis enthält als größten Posten die geplanten Personalausgaben, die wie geplant abgerufen und verausgabt wurden.

Die Inlandsdienstreisen zu den Projektmeetings wurden Durchgeführt.

Für die geplante Auslandsreise konnte zu diesem Zeitpunkt kein uns angemessen erscheinendes Paper vorbereitet werden. Ersatzweise wurde auf Kosten des IFF eine Reise zur ION ITM 2013 in San Diego durchgeführt.

Das „CAN Aufzeichnungs Device“ musste nicht beschafft werden, da ein gleichwertiges System zu diesem Zeitpunkt am IFF verfügbar war.

4.2 Notwendigkeit und Angemessenheit der geleisteten Arbeit

Als Universität’s Institut ist das IFF auf Förderungen im Rahmen von öffendlichen Förderprogrammen angewiesen. Die Arbeit wurde sorgsam geplant und im Sinne wirtschaftlichen und sparsamen Umgangs mit Fördermitteln bearbeitet. So wurde z.B. das beantragte „CAN Aufzeichnungs Device“ nicht beschafft, da ein gleichwertiges System zu diesem Zeitpunkt am IFF verfügbar war.

4.3 Voraussichtlicher Nutzen

Die Forschungsergebnisse wurden vom Projektpartner IfEN GmbH in seinen Konstellationssimulator integriert und können so zukünftig als Testsystem für eine Vielzahl an Automotive Anwendungen eingesetzt werden. Das IFF hat mit der Fähigkeit Radsensoren für eine gegebene Trajektorie zu simulieren ein Werkzeug, das bereits zur Unterstützung anderer Forschungsarbeiten im Bereich der Automatischen Führung von Feldmaschinen eingesetzt werden konnte. Die recherchierten Algorithmen wurden zur Verwendung als Stützinformation in Kopplungsfiltern weiterentwickelt.

4.4 Bekannt gewordener Fortschritt bei anderen Stellen

Fortschritte anderer Stellen die die speziellen Themen des IFF in TEGA betreffen sind nicht bekannt geworden.

4.5 Öffentlichkeitsarbeit und Veröffentlichungen

Für die geplante Auslandsreise konnte zu diesem Zeitpunkt kein uns angemessen erscheinendes Paper vorbereitet werden. Ersatzweise wurde auf Kosten des IFF eine Reise zur

Copyright © 2013, TEGA Konsortium. Alle Rechte vorbehalten.

ION ITM 2013 in San Diego durchgeführt und die Ergebnisse dort in dem Vortrag „Aiding GNSS Signal Tracking Loops Using Vehicle Dead Reckoning Sensors“ mit vorgestellt.

Copyright © 2013, TEGA Konsortium. Alle Rechte vorbehalten.

5. Zusammenfassung

Die im Rahmen des TEGA-Projekts vom IFF bearbeiteten Arbeitspakete wurden erfolgreich durchgeführt und planmäßig abgeschlossen. Die erstellten technischen Zwischenberichte beinhalten Herleitung und Validierung des angestrebten Modells.

Gefördert durch:

Bundesministerium
für Wirtschaft
und Technologie

aufgrund eines Beschlusses
des Deutschen Bundestages

Copyright © 2013, TEGA Konsortium. Alle Rechte vorbehalten.

6. Literaturverzeichnis

[B.1] N. N. Department of defence, world geodetic system 1984, its definition and relationshipswith local geodetic systems. Technical report, National Imagery and Mapping Agency, NIMA, January 2000

[B.2] Cai, Guowei, Chen, Ben M., Lee, Tong Heng, Unmanned Rotorcraft Systems, Springer, ISBN 978-0-85729-634-4

[B.3] Reif, Konrad, Bosch-Autoelektrik und –Autoelektronik, Bordnetze, Sensoren und elektronische Systeme, Vieweg + Teubner 2011, ISBN 3834812749

[B.4] Bonnifait, P. et al., Data Fusion of Four ABS Sensors and GPS for an Enhanced Localization of Car-like Vehicles, Proceedings of the 2001 IEEE International Conference on Robotics & Automation Seoul, Korea. May 21-26, 2001

[B.5] Godha, S.; Cannon, M. E.; GPS/MEMS INS integrated system for navigation in urban areas, GPS/MEMS INS integrated system for navigation in urban areas

[B.6] Gao, J.; Petovello, M.G.; Cannon, M.E.; Development of Precise GPS/INS/Wheel Speed Sensor/Yaw Rate Sensor Integrated Vehicular Positioning System, ION NTM 2006, 18-20 January 2006, Monterey, CA

[B.7] Persson, N.; Event Based Sampling with Application to Spectral Estimation, Linköping Studies in Science and Technology, Thesis No. 981, 2002

Copyright © 2013, TEGA Konsortium. Alle Rechte vorbehalten.

A TN 5: Vehicle Navigation Algorithms

A.1 Introduction

A.1.1 Scope of the Document

This document covers the results of the TEGA AP 3200 “Theoretische Modellierung 'Fahrzeugdynamik'”. This document provides the algorithms to simulate an experimental test platform under consideration of realistic vehicle dynamics.

A.2 Fundamental System Description

A.2.1 Introduction

The following paragraphs are containing the basic vehicle description. Geometrical properties as well as the sensors that the vehicle uses are described in this paragraph. Furthermore, the underlying assumptions about the vehicle’s movement are elaborated on in this section.

A.2.2 General Assumptions

Generally, the following formulas and algorithms are applicable for the type of automobile described in this paragraph.

- A typical passenger car is modeled in the following algorithms. It has four wheels of which the two front wheels are steered using an Ackermann steering geometry
- It is assumed that the vehicle is a rigid body apart from the spinning wheels and the steered front axle. That means that there is no relative translational motion between the wheels and the chassis
- The vehicle tends to move in a horizontal plane. Vertical movement is relatively small compared to horizontal movement
- As a result of the horizontal movement, pitch and roll of the vehicle are small angles
- The no slip condition between wheels and surface is granted at all times
- In case the roll angle is not known from a reference input trajectory, it is assumed to be zero.
- It is assumed that the trajectory is smooth and continuous

Copyright © 2013, TEGA Konsortium. Alle Rechte vorbehalten.

A.2.3 Reference Systems

A.2.3.1 Global WGS 84 Coordinate System

In order to define a position globally, this document will refer to the commonly used WGS84 coordinate system. It defines an ellipsoidal system that is flattened at the poles. The following parameters of the WGS84 ellipsoid can be found in [B.1].The parameters provide the basis for several transformations within the vehicle kinematic equations.

Tab. 3: WGS84 parameters

Semimajor axis A_{WGS}	6378137.0 m
Semiminor axis B_{WGS}	6356752.31425 m
Eccentricity e	8.1819190842622 10^{-2}
Flattening f	1/298.257223563
Angular velocity Ω_E	7292115 * 10-11 rad/s
Geocentric gravitational constant GM_E	3986004.418 *10^8 m^3/s^2

The position is expressed as the geodetic latitude (φ), geodetic longitude (λ) and the height above the ellipsoid (h).

The relationship between the Cartesian “Earth Centered Earth Fixed” and the geodetic latitude, longitude and altitude is given in the following equations:

$$x = (N+h)\cos\varphi\cos\lambda$$
$$y = (N+h)\cos\varphi\sin\lambda$$
$$z = \left[N(1-e^2)+h\right]\sin\varphi$$

with

$$N = \frac{a}{\sqrt{1-e^2\sin^2\varphi}}$$

Copyright © 2013, TEGA Konsortium. Alle Rechte vorbehalten.

A.2.3.2 Local North East Down (NED) Coordinate System

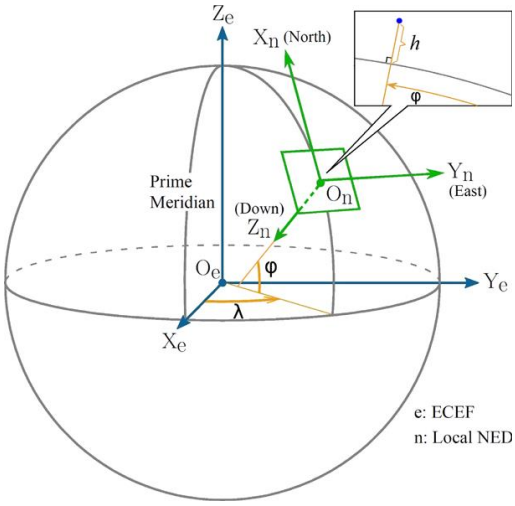

Abb. 4: NED coordinate system [B.2]

The x-y-plane of the local NED coordinate system is parallel to the earth's surface. Based on the WGS84 ellipsoid model it can be defined by the following properties:

- The origin can be arbitrarily chosen
- The x-axis points toward the ellipsoid north (geodetic north)
- The y-axis points toward the ellipsoid east (geodetic east)
- The z-axis points downward along the ellipsoid normal

Within the scope of this document, the origin of the NED-system is defined in the center of the vehicles rear axle unless otherwise stated.

In order to rotate a vector from ECEF to NED, the following relationship applies:

$$\vec{v}_{NED} = \begin{pmatrix} -\sin\varphi\cdot\cos\lambda & -\sin\varphi\cdot\sin\lambda & \cos\varphi \\ -\sin\lambda & \cos\lambda & 0 \\ -\cos\varphi\cdot\cos\lambda & -\cos\varphi\cdot\sin\lambda & -\sin\varphi \end{pmatrix} \cdot \vec{v}_{ECEF} \qquad (6\text{-}1)$$

Copyright © 2013, TEGA Konsortium. Alle Rechte vorbehalten.

A.2.3.3 Vehicle fixed Coordinate System

The vehicle-fixed coordinate system is directly defined on the body of the automobile. Its origin and axes are defined as follows:

- The origin is located at the center if the rear axle of the vehicle and marks the reference point of the vehicle's motion
- The x-axis points forward, is lying in the symmetric plane vehicle and intersects the front axle
- The y-axis points along the rear axle to the right of the vehicle
- The z-axis points downward perpendicular to the x-y-plane

The Euler angles roll Φ, pitch Θ and yaw Ψ define the orientation of the vehicle fixed coordinate system relative to the NED system. In order to rotate a vector from NED to vehicle-fixed, the following relationship applies:

$$\vec{v}_b = \begin{pmatrix} \cos\Theta\cdot\cos\Psi & \cos\Theta\cdot\sin\Psi & -\sin\Theta \\ \sin\Phi\cdot\sin\Theta\cdot\cos\Psi-\cos\Phi\cdot\sin\Psi & \sin\Phi\cdot\sin\Theta\cdot\sin\Psi+\cos\Phi\cdot\cos\Psi & \sin\Phi\cdot\cos\Theta \\ \cos\Phi\cdot\sin\Theta\cdot\cos\Psi+\sin\Phi\cdot\sin\Psi & \cos\Phi\cdot\sin\Theta\cdot\sin\Psi-\sin\Phi\cdot\cos\Psi & \cos\Phi\cdot\cos\Theta \end{pmatrix}\cdot\vec{v}_{NED} \quad \textbf{(6-2)}$$

Copyright © 2013, TEGA Konsortium. Alle Rechte vorbehalten.

A.3 Fundamentals of the vehicle's motion

A.3.1 Geometry of the Vehicle

As mentioned in A.2.2, the kinematic model used within the TEGA Project is based on a four-wheel-vehicle. The wheels are rigidly connected to the vehicle body besides the rotational movement and the steering angle. A suspension is neglected for this application. The model is symmetrical about the vehicle body's longitudinal axis. The front wheels steered according to the Ackermann steering model. The vehicle motion is constrained to planar movements only. The rear wheels are not steered and are aligned with the longitudinal axis of the vehicle-fixed coordinate system.

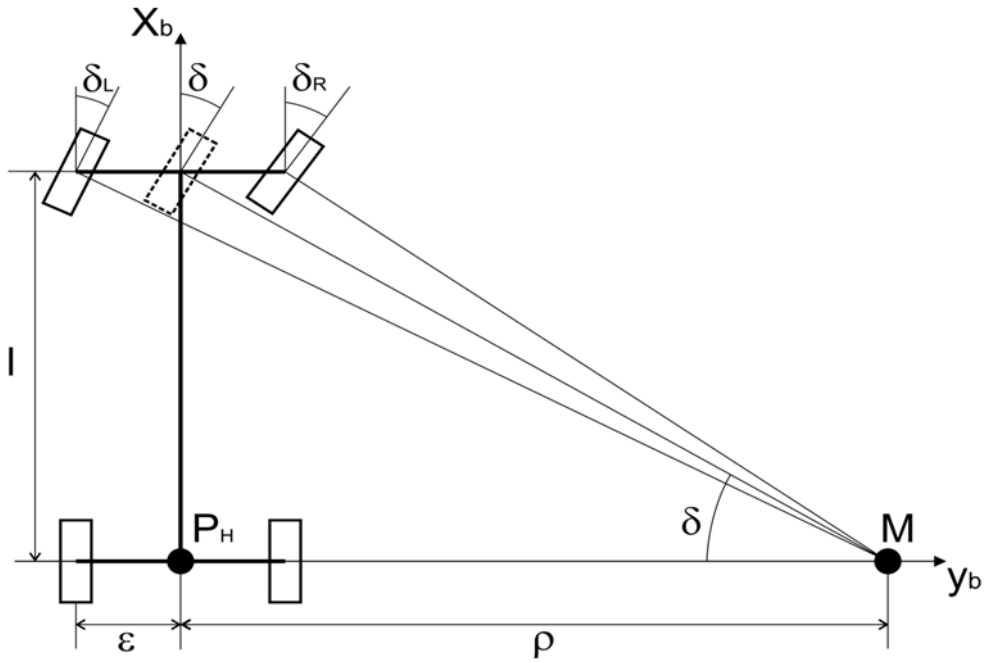

Abb. 5: View of the vehicles x-y-plane

The vehicle geometry is mainly defined by two parameters. The half track ε is the distance between the centerline of one wheel and the middle of the axle. The wheelbase l is the distance between the front and the rear axles. The plane of the vehicle's movement is inclined with Θ towards the horizontal plane.

Typically, the sensors that are integrated in a vehicle are a longitudinal acceleration sensor, a gyroscope measuring the yaw rate, wheel speed sensors for all wheels as well as a steering wheel angle sensor.

Copyright © 2013, TEGA Konsortium. Alle Rechte vorbehalten.

It has been defined at the KOM of the project, that the trajectory of the vehicle's reference point is given as the discretized position (x, y, z) and the consistent velocity (v_x, v_y, v_z) in Cartesian ECEF coordinates with a corresponding timestamp.

A.3.2 Definition of the Vehicle's Euler Angles

However, the movement of the reference point does not contain any attitude information so that the roll, pitch and yaw angle need to be modeled.

The roll angle is assumed to be insignificantly small. A modeling of this angle requires a detailed terrain model which is not in the scope of this project and cannot be derived from the vehicle's model by itself. Additionally, the impact of the roll angle on the desired sensor measurements is relatively small so that it can be neglected without a negative impact on the project results.

The pitch angle Θ and the heading or yaw angle Ψ can directly be derived from the trajectory of the reference point as it can be assumed that the vehicle moves along the x-axis of the vehicle-fixed coordinate system.

After transforming the velocity from ECEF to NED following equation (6-1), the pitch and yaw information can be derived by:

$$\Psi = \tan^{-1}\left(\frac{v_E}{v_N}\right) \tag{6-3}$$

$$\Theta = \tan^{-1}\left(-\frac{v_D}{\sqrt{v_N^2 + v_E^2}}\right) \tag{6-4}$$

These non-holonomic constrains are widely accepted in the scientific community, i.e. see [B.4], [B.5] or [B.6].

A.3.3 Track Curvature and Yaw Rate

It can be derived from Abb. 5 that the local curvature of the driven track plays an essential role in the definition of the steering angle and the wheel speeds. However, it is not part of the trajectory input file and needs to be calculated. Three options for calculating the curvature will be presented.

Copyright © 2013, TEGA Konsortium. Alle Rechte vorbehalten.

A.3.3.1 Option 1a

The vehicles incremental movement can be understood as a two dimensional motion within the x-y-plane of the vehicle fixed coordinate system. It is therefore of interest to calculate the curvature along the track within this plane.

At every point of the track the curvature can be approximated by osculating circles. The following equation (6-5) defines the two dimensional curvature of an osculating circle as

$$\kappa(\tau)=\frac{1}{\rho(\tau)}=\frac{\dot{x}(\tau)\cdot\ddot{y}(\tau)-\ddot{x}(\tau)\cdot\dot{y}(\tau)}{\sqrt{\left(\dot{x}(\tau)^2+\dot{y}(\tau)^2\right)^3}} \qquad \textbf{(6-5)}$$

The first and second derivative of the coordinates $(x,y)_b$ are also not part of the trajectory file. They can be approximated by pseudo-differencing the trajectory file as $\Delta\tau$ is small and can be cancelled out from the derivatives.

The first step is to generate a list of the coordinate differences for $(x,y,z)_{ECEF}$ such as

$$\begin{aligned}\dot{x} &\approx x_{k+1}-x_k\\ \dot{y} &\approx y_{k+1}-y_k\\ \dot{z} &\approx z_{k+1}-z_k\end{aligned} \qquad \textbf{(6-6)}$$

If the trajectory file contains n entries, the list will obviously shortened to $(n-1)$.

Similarly generate a list of the second derivative, the list will be shortened to $(n-2)$:

$$\begin{aligned}\ddot{x} &\approx \dot{x}_{k+1}-\dot{x}_k\\ \ddot{y} &\approx \dot{y}_{k+1}-\dot{y}_k\\ \ddot{z} &\approx \dot{z}_{k+1}-\dot{z}_k\end{aligned} \qquad \textbf{(6-7)}$$

Copyright © 2013, TEGA Konsortium. Alle Rechte vorbehalten.

The first and second derivative vectors $\dot{\vec{x}}_{ECEF}$ and $\ddot{\vec{x}}_{ECEF}$ then need to be transformed into the vehicle-fixed coordinate system using (6-1) and (6-2) at the respective coordinates. Then for every time step k the curvature κ can be obtained using the x and y components of $\dot{\vec{x}}_b(k)$ and $\ddot{\vec{x}}_b(k)$ in (6-5).

$$\kappa(k) = \frac{1}{\rho(k)} = \frac{\dot{x}_b \cdot \ddot{y}_b - \ddot{x}_b \cdot \dot{y}_b}{\sqrt{\left(\dot{x}_b^2 + \dot{y}_b^2\right)^3}} \tag{6-8}$$

The yaw rate $\dot{\Psi}$ can then be derived from the velocity V of the reference point and the local curvature of the track:

$$\begin{aligned} \dot{\Psi} \cdot \cos\Theta &= \frac{V}{\rho} = V \cdot \kappa \\ \Leftrightarrow \dot{\Psi} &= \frac{V \cdot \kappa}{\cos\Theta} \end{aligned} \tag{6-9}$$

A.3.3.2 Option 1b

Similarly to Option 1a the following procedure is based on equation (6-5). The major difference is that the curvature is not derived from the position $(x, y, z)_{ECEF}$ but from the velocities. Equation (6-8) is modified to

$$\kappa(k) = \frac{1}{\rho(k)} = \frac{v_x^b \cdot \dot{v}_y^b - v_y^b \cdot \dot{v}_x^b}{\sqrt{\left(\left(v_x^b\right)^2 + \left(v_y^b\right)^2\right)^3}} \tag{6-10}$$

With the velocity $\vec{v}^{\,b}$ in vehicle-fixed coordinates and

Copyright © 2013, TEGA Konsortium. Alle Rechte vorbehalten.

$$\dot{v}_x^b \approx \frac{v_{x,k+1}^b - v_{x,k}^b}{t_{k+1} - t_k}$$
$$\dot{v}_y^b \approx \frac{v_{y,k+1}^b - v_{y,k}^b}{t_{k+1} - t_k} \quad \textbf{(6-11)}$$

A.3.3.3 Option 2

In the second option it is assumed that $\dot{\Psi}$ is known from the trajectory by using

$$\dot{\Psi} \approx \frac{\Psi_{k+1} - \Psi_k}{t_{k+1} - t_k} \quad \textbf{(6-12)}$$

Based on (6-9) the curvature κ can be calculated using.

$$\kappa = \frac{\dot{\Psi} \cdot \cos\Theta}{V} \quad \textbf{(6-13)}$$

The choice on either of these options may be based on the noise levels of the data in the trajectory.

A.3.4 Longitudinal Acceleration

The longitudinal acceleration can be approximated by differencing the vehicle speed from the trajectory file:

$$\dot{V} \approx \frac{|\vec{v}_{k+1}| - |\vec{v}_k|}{t_{k+1} - t_k} \quad \textbf{(6-14)}$$

Copyright © 2013, TEGA Konsortium. Alle Rechte vorbehalten.

A.3.5 Wheel Speeds and Steering Angle

Based on the velocity of the vehicle's reference point and the local curvature of the track the velocities of all wheels can be defined:

$$V_{HL} = V \cdot \left(1 + \frac{\varepsilon}{\rho}\right) = V \cdot \left(1 + \varepsilon \cdot \kappa\right) \tag{6-15}$$

$$V_{HR} = V \cdot \left(1 - \frac{\varepsilon}{\rho}\right) = V \cdot \left(1 - \varepsilon \cdot \kappa\right) \tag{6-16}$$

$$V_{VL} = V \cdot \sqrt{1 + 2 \cdot \frac{\varepsilon}{\rho} + \frac{1}{\rho^2} \cdot \left(l^2 + \varepsilon^2\right)} = V \cdot \sqrt{1 + 2 \cdot \varepsilon \cdot \kappa + \kappa^2 \cdot \left(l^2 + \varepsilon^2\right)} \tag{6-17}$$

$$V_{VR} = V \cdot \sqrt{1 - 2 \cdot \frac{\varepsilon}{\rho} + \frac{1}{\rho^2} \cdot \left(l^2 + \varepsilon^2\right)} = V \cdot \sqrt{1 - 2 \cdot \varepsilon \cdot \kappa + \kappa^2 \cdot \left(l^2 + \varepsilon^2\right)} \tag{6-18}$$

Furthermore, the steering angle of the virtual front wheel is given by

$$\delta = \tan^{-1}\left(\frac{l}{\rho}\right) = \tan^{-1}\left(l \cdot \kappa\right). \tag{6-19}$$

If required, the steering angles of the front wheels can also be calculated [B.4]:

$$\delta_L = \tan^{-1}\left(\frac{l \cdot \tan\delta}{l + \varepsilon \cdot \tan\delta}\right) \tag{6-20}$$

$$\delta_R = \tan^{-1}\left(\frac{l \cdot \tan\delta}{l - \varepsilon \cdot \tan\delta}\right) \tag{6-21}$$

Copyright © 2013, TEGA Konsortium. Alle Rechte vorbehalten.

A.4 Vehicle Dynamic Sensors

A.4.1 Wheel Speed Sensors

Wheel speed sensors are commonly used in current vehicles for antilock and stability systems. Also route guidance systems obtain the information from these sensors.

The current typical set up consists of a pulse encoder that is fixed to the wheel hub. It has the same angular velocity as the wheel. The encoder induces a pulse at a static sensor head. The signal is then processed, digitized and the data is transmitted to a control unit.

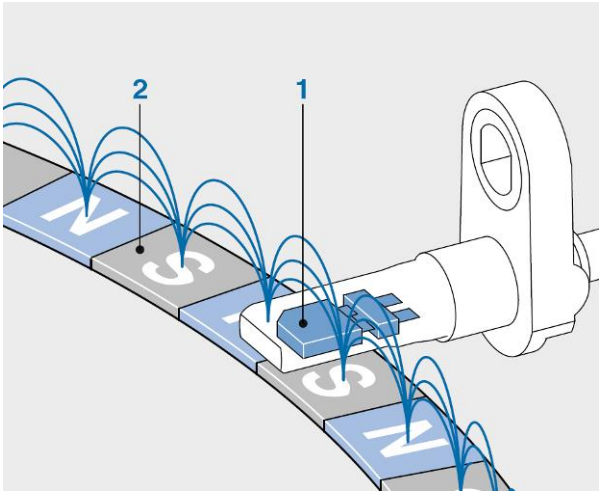

Abb. 6: Schematic of a wheel speed sensor [B.3]

A.4.1.1 Output as Number of Pulses

The relationship between the velocity V_i and the number of pulses n_i at the wheel is defined as

$$V_i = \frac{n_i}{n_{2\pi}} \cdot \frac{2\pi \cdot r_i}{\Delta t_i} \qquad \textbf{(6-22)}$$

where r_i is the radius of the wheel, $n_{2\pi}$ is the number of pulses for one full rotation and Δt_i is the time interval in which the number of pulses have been counted. Solving equation (6-22) for the number of pulses n_i delivers

Copyright © 2013, TEGA Konsortium. Alle Rechte vorbehalten.

$$n_i = V_i \cdot n_{2\pi} \cdot \frac{\Delta t_i}{2\pi \cdot r_i}. \qquad \textbf{(6-23)}$$

The number of pulses n_i is an integer value which by itself defines the quantization.

When calculating a velocity from the number of pulses, a common error source is the scale factor error that is regularly a result of variation in the radius of the wheel. It can be considered by applying

$$r_i = a_{WS,i} \cdot r_0 \qquad \textbf{(6-24)}$$

with $a_{WS,i}$ being the scale factor error and r_0 the nominal radius of the wheel.

A.4.1.2 Output as a Velocity Value

It is also common, that the wheel speeds are passed to the CAN-Bus as (discretized) float values in m/s or km/h. In this case, the data processing integrated in the sensor already calculates the velocity values with an anticipated wheel radius. As the sensor production in reality is not absolutely precise, the teeth inducing the pulses are not evenly spaced. This typically results in a periodic error as illustrated in the following Abb. 7:

Copyright © 2013, TEGA Konsortium. Alle Rechte vorbehalten.

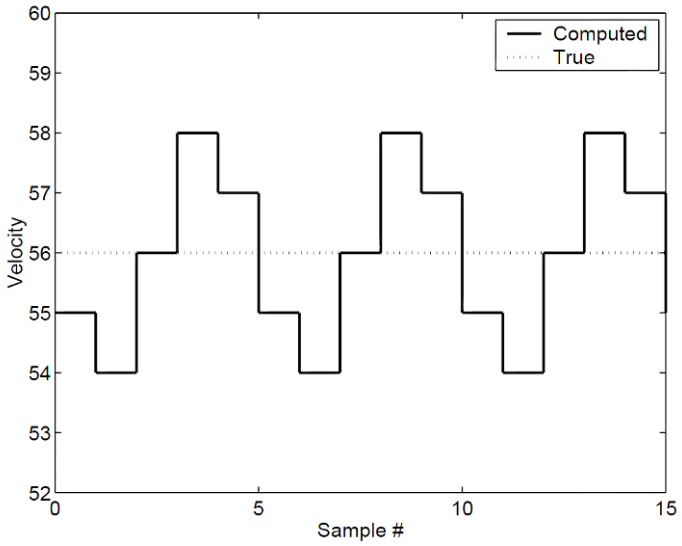

Abb. 7: Periodic Error of Wheel Speed Sensors [B.7]

As the periodic error is a result of the geometric properties of the sensor, its frequency is a result of the speed of the wheel. The following figures illustrate that behavior:

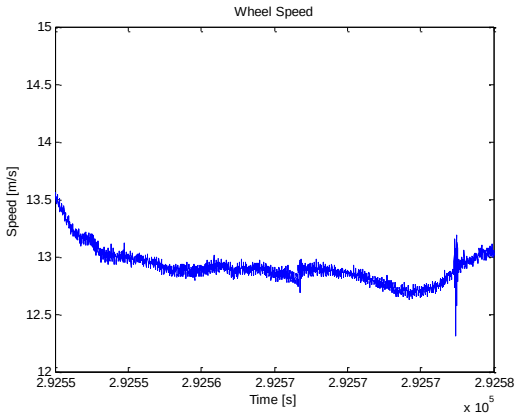

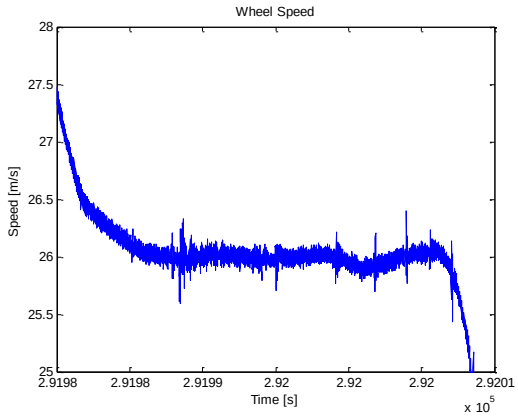

Copyright © 2013, TEGA Konsortium. Alle Rechte vorbehalten.

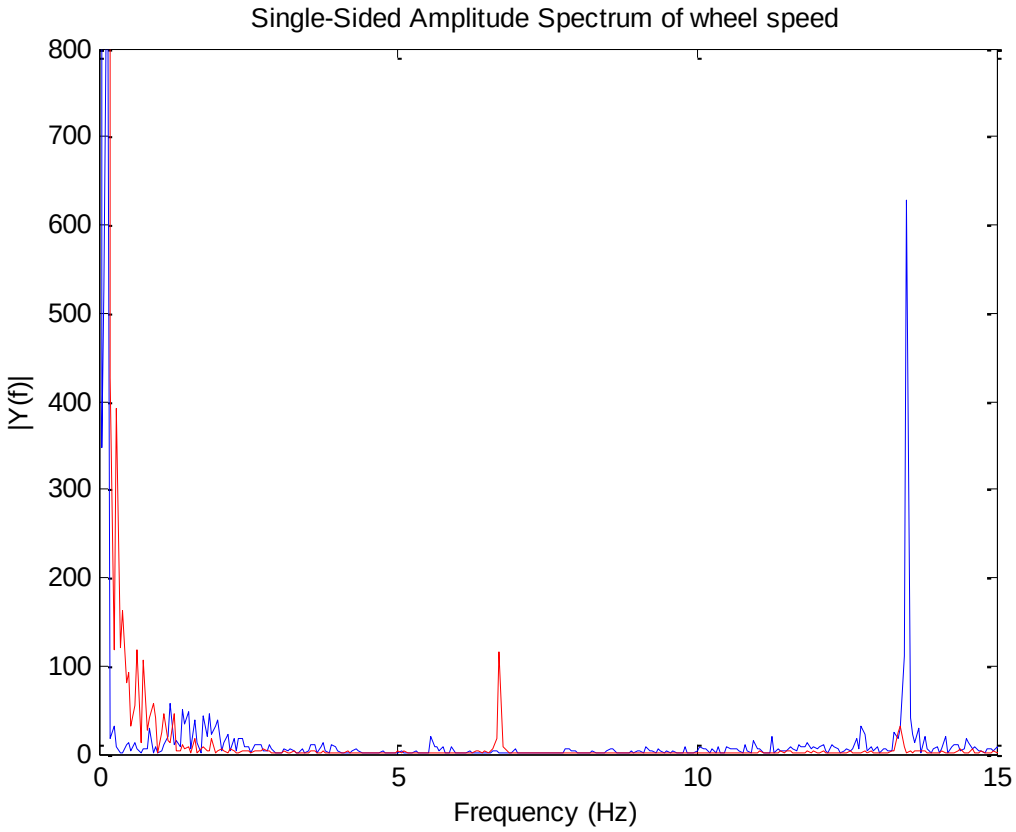

Abb. 8: FFT of the Periodic Wheel Speed Error

The upper figures show a plot of the wheel speeds of the institute's test vehicle over time at two approximately constant speeds. The left figure shows a speed of ~13 m/s, the speed in the right plot is approximately twice as fast (~26 m/s). These velocities in these periods have been Fourier transformed. The spectrum is plotted in the lower chart of Abb. 8. The red line corresponds to the lower speed, the blue line to the faster speed.

It can be observed, that when the speed doubles, the frequency also doubles (6.7 Hz vs.13.5 Hz). When taking into account that the circumference of the wheel is approx. 1.92 m the corresponding angular rates of the wheel speed sensors are:

$$f_{13\text{m/s}} = \frac{13\,\frac{\text{m}}{\text{s}}}{1.92\,\text{m}} = 6.77\,\text{Hz}$$

Copyright © 2013, TEGA Konsortium. Alle Rechte vorbehalten.

$$f_{26\,\mathrm{m/s}} = \frac{26\,\frac{\mathrm{m}}{\mathrm{s}}}{1.92\,\mathrm{m}} = 13.54\,\mathrm{Hz}$$

In this case, the frequency of the periodic error correlates with the angular rate of the wheel.

The estimated velocity $V_{i,est}$ can then be approximated by

$$V_{i,est} = a_{WS,i} \cdot \left(V_i + a_{PE,i} \cdot \cos\left(\frac{V_i}{r_0} \cdot t \right) \right) \qquad \textbf{(6-25)}$$

with $a_{WS,i}$ again being the scale factor error by which the estimated wheel radius differs from the true radius. The amplitude of the periodic error is given in $a_{PE,i}$. The time t is a continuous time with an arbitrarily chosen starting point.

In this case, the quantization and noise however are typically not a result of the sensor resolution. The quantization ΔV is defined by the measurement range and the number of bits reserved for message:

$$\Delta V = \frac{V_u - V_l}{2^q} \qquad \textbf{(6-26)}$$

In this case ΔV are the velocity increments and q is the number of bits that are used for encoding the message. V_u and V_l are the upper and lower bounds of the measurement range. Typically $V_l = 0$ applies for wheel speed sensors.

The measurement value of the vehicle speed is then defined as

Copyright © 2013, TEGA Konsortium. Alle Rechte vorbehalten.

$$V_{i,meas} = \Delta V \cdot \text{round}\left(\frac{V_{i,est} + \varepsilon_V}{\Delta V}\right) \quad \textbf{(6-27)}$$

with ε_V being white noise on the estimated velocity. Note that $V_l \leq V_{i,meas} \leq V_u$.

A.4.2 Acceleration Sensors

Acceleration sensors in automobiles are typically designed as Hall- or MEMS-Sensors. Commonly a mass-spring system is used for detecting acceleration.

Abb. 9: MEMS acceleration sensor [B.3]

As the sensitive axis of the sensor is typically not perfectly aligned with the longitudinal axis of the vehicle, the following equation applies for the resulting acceleration projected on the sensitive axis:

$$\dot{V}_{sense} = \dot{V} + g \cdot \sin(\Theta + \delta\Theta) + \dot{\Psi} \cdot V \cdot \sin(\delta\Psi) \quad \textbf{(6-28)}$$

The gravitational acceleration is defined as g. The angles $\delta\Theta$ and $\delta\Psi$ are the alignment errors by which the sensitive axis of the accelerometer differs from the respective axes of the vehicle-fixed coordinate system. It can be derived from (6-28) that $\delta\Theta$ can be understood as a

Copyright © 2013, TEGA Konsortium. Alle Rechte vorbehalten.

part of the bias error that is typical for accelerometers. Hence the estimated value for the longitudinal acceleration can be defined as

$$\dot{V}_{est} = a_{acc} \cdot \left(\dot{V} + g \cdot \sin(\Theta) + \dot{\Psi} \cdot V \cdot \sin(\delta\Psi)\right) + b_{acc} \qquad \textbf{(6-29)}$$

For further ease of implementation it can commonly be assumed that $\delta\Psi$ is very small and the centripetal acceleration does have no significant influence on the measurement of $\dot{V}$, delivering

$$\dot{V}_{est} = a_{acc} \cdot \left(\dot{V} + g \cdot \sin(\Theta)\right) + b_{acc} \qquad \textbf{(6-30)}$$

After quantization the measurement value yields

$$\dot{V}_{meas} = \Delta\dot{V} \cdot \text{round}\left(\frac{\dot{V}_{est} + \varepsilon_{\dot{V}}}{\Delta\dot{V}}\right) \qquad \textbf{(6-31)}$$

with $\varepsilon_{\dot{V}}$ being white noise on the estimated acceleration. The quantization $\Delta\dot{V}$ is obtained analogously to (6-26).

A.4.3 Gyroscope

Gyroscopes are typically used for stability programs to detect discrepancies in the yaw rate and the speed of the wheels that are a potential indicator for instable cornering. Gyroscopes are in this case often designed as MEMS devices.

Copyright © 2013, TEGA Konsortium. Alle Rechte vorbehalten.

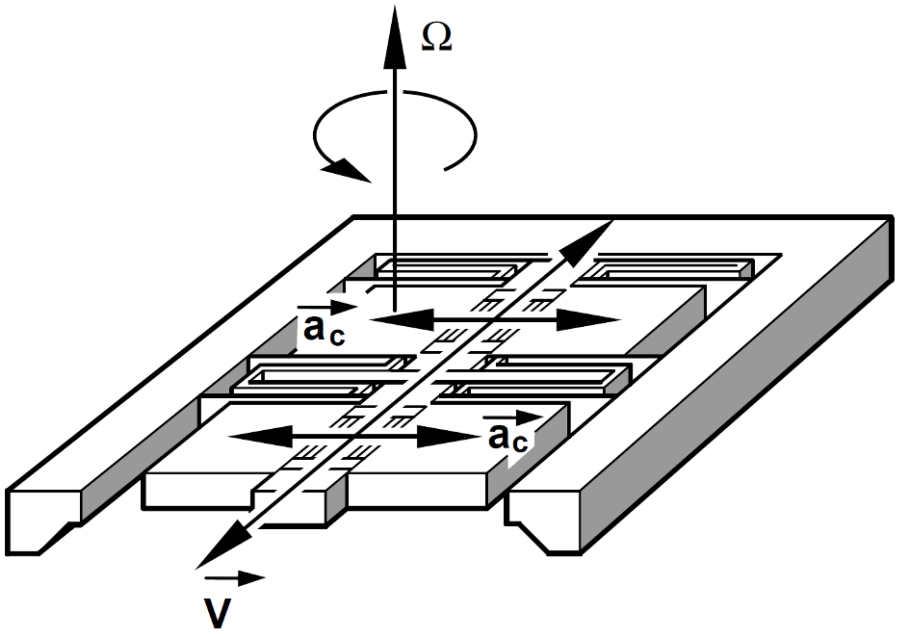

Abb. 10: Schematic of a gyroscope [B.3]

They are based on the Coriolis effect. The displacement of an oscillator gets deflected when the gyroscope is exposed to an angular velocity. The deflection is measured and the angular velocity can be calculated.

Similarly to the accelerometer the angular rate sensor is normally not perfectly aligned with the vehicle's z-axis. Thus the sensitive axis of the sensor only measures part of the angular rate. The resulting equation can be approximated as follows:

$$\dot{\Psi}_{sense} \approx \dot{\Psi} \cdot \cos(\Theta) \cdot \cos(\delta\gamma) \qquad \textbf{(6-32)}$$

The influence of the earth's rotation is insignificantly small and therefore neglected in this relationship. The influence of the misalignment $\delta\gamma$ can be merged with the scale factor error that is a regular systematical error of gyroscopes. The equation for the estimated yaw rate before quantization yields:

Copyright © 2013, TEGA Konsortium. Alle Rechte vorbehalten.

$$\dot{\Psi}_{est} = a_{yaw} \cdot \dot{\Psi} \cdot \cos(\Theta) + b_{yaw} \quad \textbf{(6-33)}$$

Again after quantization and considering noise in the signal processing chain, the measurement value $\dot{\Psi}_{meas}$ yields

$$\dot{\Psi}_{meas} = \Delta\dot{\Psi} \cdot \text{round}\left(\frac{\dot{\Psi}_{est} + \varepsilon_{\dot{\Psi}}}{\Delta\dot{\Psi}}\right) \quad \textbf{(6-34)}$$

with $\varepsilon_{\dot{\Psi}}$ being white noise on the estimated yaw rate and $\Delta\dot{\Psi}$ being the quantization.

A.4.4 Steering Wheel Sensor

To measure the steering wheel angle of a vehicle generally any kind of angle sensor can be used. Common implementations are potentiometers, optical sensors as well as sensors based on magnetic principles.

It may be advantageous to choose a sensor principle that allows a direct reading of the angular value at any time. This is not the case for sensors that incrementally calculate the steering wheel angle. As the range of potential steering wheel angles is typically ±720° or more, geared sensors are common.

One typical implementation is using magnetic elements that are not symmetrically distributed coding disk. For varying angles varying combinations of magnetic elements are measured by Hall sensors.

Copyright © 2013, TEGA Konsortium. Alle Rechte vorbehalten.

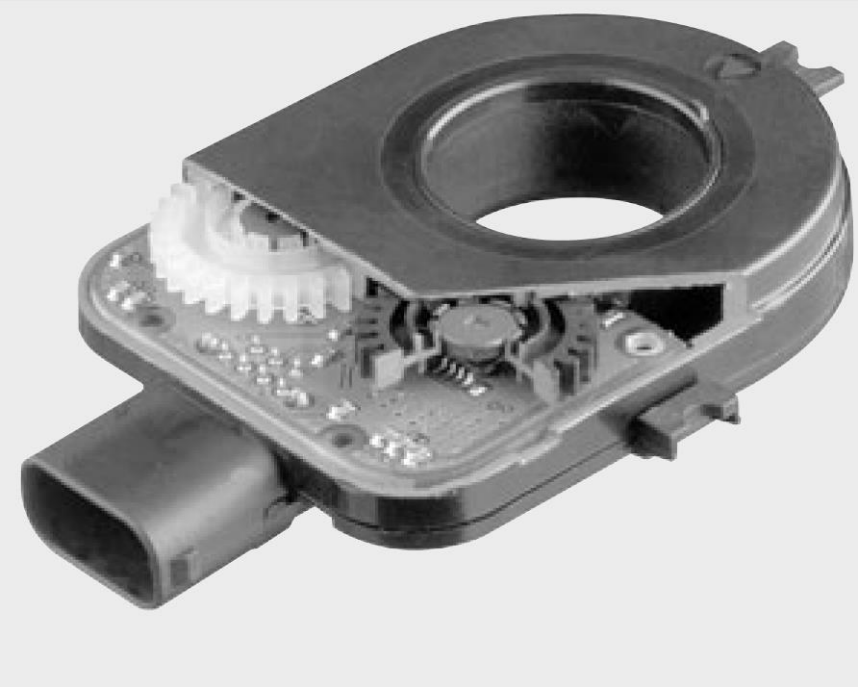

Abb. 11: Steering wheel sensor [B.3]

The relationship between steering wheel angle and steering angle of the virtual front wheel can typically be described by a polynomial. The respective equation gives

$$\alpha_{SW,est} = \sum_{i=0}^{n} a_i \cdot \delta^i \,. \qquad \textbf{(6-35)}$$

Note that the polynomial must be bijective, otherwise a distinct mapping of steering wheel angles on steering angles would not be possible. Typically the order of the polynomial does not exceed the third order. A simple example would be a linear relationship between steering wheel angle α_{SW} and steering angle δ. Assuming that the maximum steering wheel angle $\alpha_{SW,\max} = \pm 720°$ and the maximum steering angle $\delta_{\max} = \pm 30°$ the corresponding relationship following (6-35) would yield

$$\alpha_{SW,est} = 24 \cdot \delta \,. \qquad \textbf{(6-36)}$$

Copyright © 2013, TEGA Konsortium. Alle Rechte vorbehalten.

The measured steering wheel angle $\alpha_{SW,meas}$ can then be calculated from

$$\alpha_{SW,meas} = \Delta\alpha \cdot \text{round}\left(\frac{\alpha_{est} + \varepsilon_{\alpha}}{\Delta\alpha}\right) \quad \textbf{(6-37)}$$

Although noise is typically not an issue with steering wheel sensors it is considered in this equation. Again, the quantization $\Delta\alpha$ follows the general assumption as described in (6-26).

Copyright © 2013, TEGA Konsortium. Alle Rechte vorbehalten.

A.5 Validation of Algorithms

In order to prove that the described algorithms are valid for vehicle applications they have been evaluated with a demo scenario. This evaluation is to be understood as a supplement to WP 3500 ensuring that the algorithms are confirmed before they are implemented in the final system.

A.5.1 Geometric Track Properties

To allow a comprehensible assessment of the algorithm a circular reference track has been generated including position and velocity in ECEF Cartesian coordinates. It is a horizontal track with a radius of 200 m and a velocity of 20 m/s. The movement in the x-y-plane of an NED coordinate system is shown in Abb. 12.

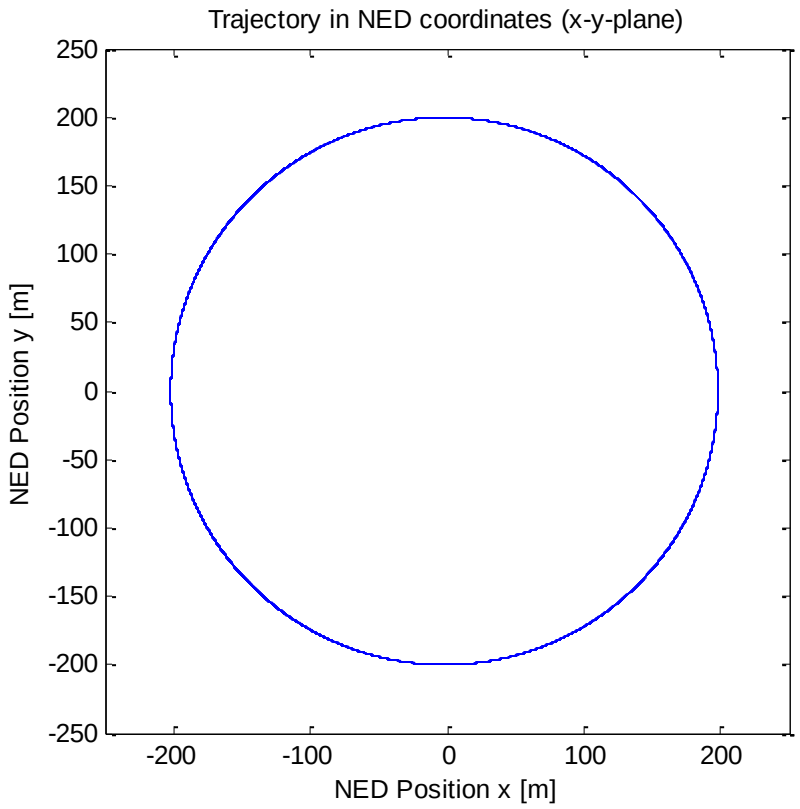

Abb. 12: Trajectory used for evaluating the vehicle kinematic algorithms

The following Abb. 13 shows the pitch angle and the heading over time of the circular movement. The pitch angle shows a little oscillation that is a result of the planar motion plotted in local NED coordinates as the local horizontal plane can be inclined towards the planar circular movement. The heading angle changes at a constant angular speed in the counter clockwise direction which is indicated by the sawtooth function with a negative slope.

Copyright © 2013, TEGA Konsortium. Alle Rechte vorbehalten.

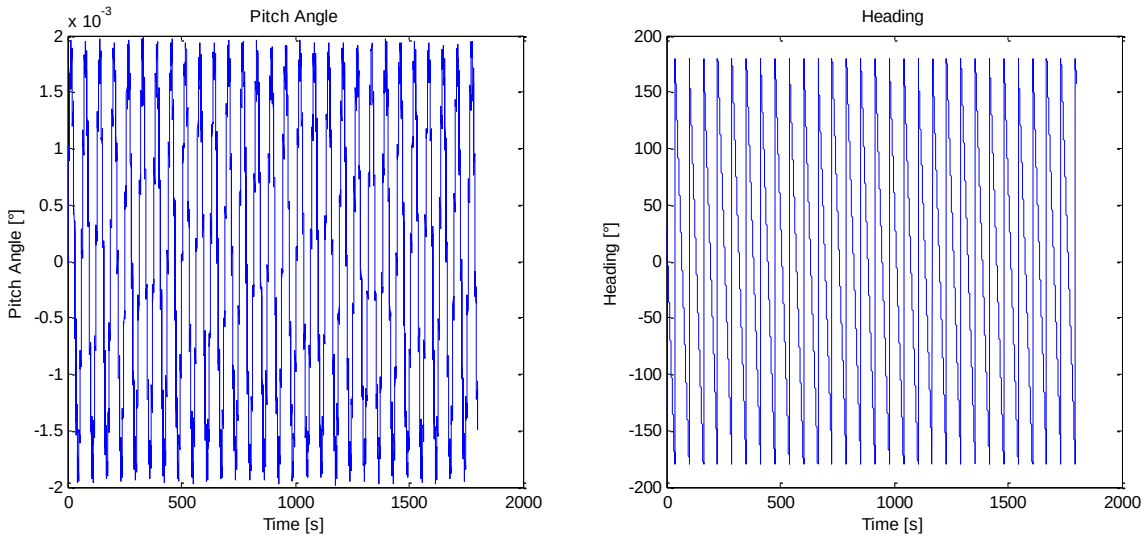

Abb. 13: Pitch and heading of the planer motion

Based on the trajectory the local radius of the track has been derived following the two options described in chapter A.3.3. The following Abb. 14 shows the results for the estimated curvature of the circular track using Option 1a (see chapter A.3.3.1). It can be observed that on average the radius is estimated accurately yielding a mean value of -199.998 m (the negative sign is a result of the counter-clockwise movement). The noise of the radius estimation is in this case $\sigma_{\text{Radius,Option1a}} = 0.7116\,\text{m}$.

Copyright © 2013, TEGA Konsortium. Alle Rechte vorbehalten.

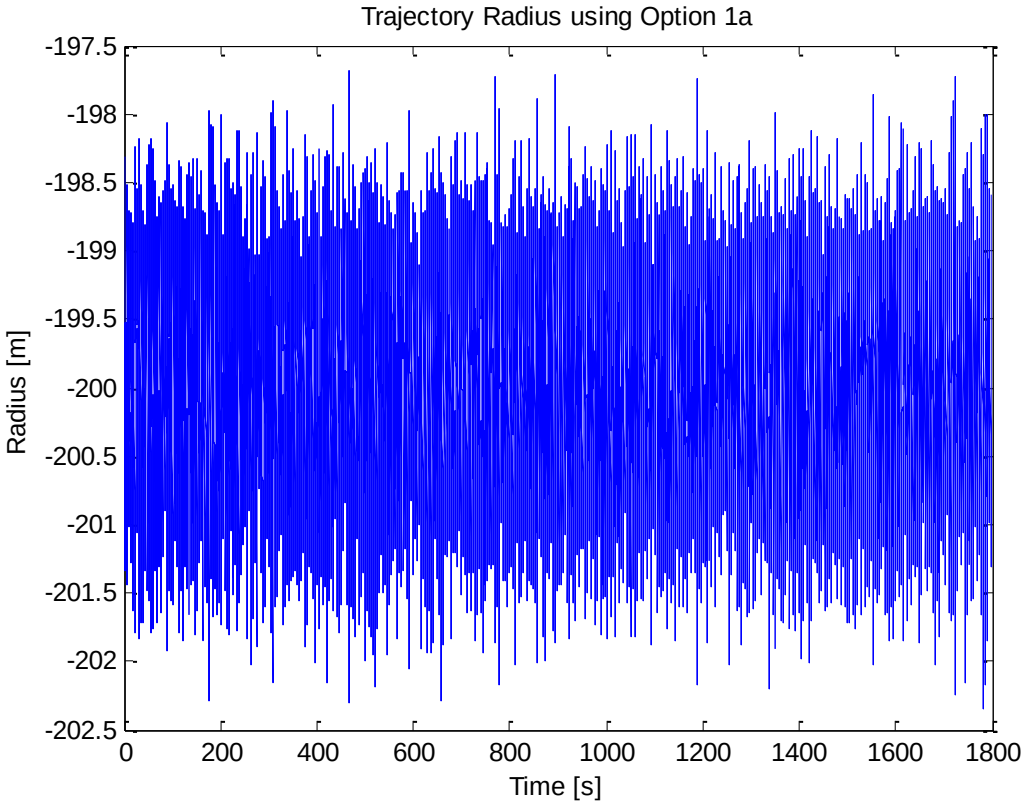

Abb. 14: Estimated radius of the circular track using option 1a

The following Abb. 15 is a plot of the results for the estimated curvature of the track using Option 1b (see chapter A.3.3.2). In this case the average the radius is again estimated accurately yielding a mean value of -200.0033 m. The noise of the radius estimation is $\sigma_{\text{Radius,Option1b}} = 0.0414\,\text{m}$ which is significantly less than the noise of option 1a.

Copyright © 2013, TEGA Konsortium. Alle Rechte vorbehalten.

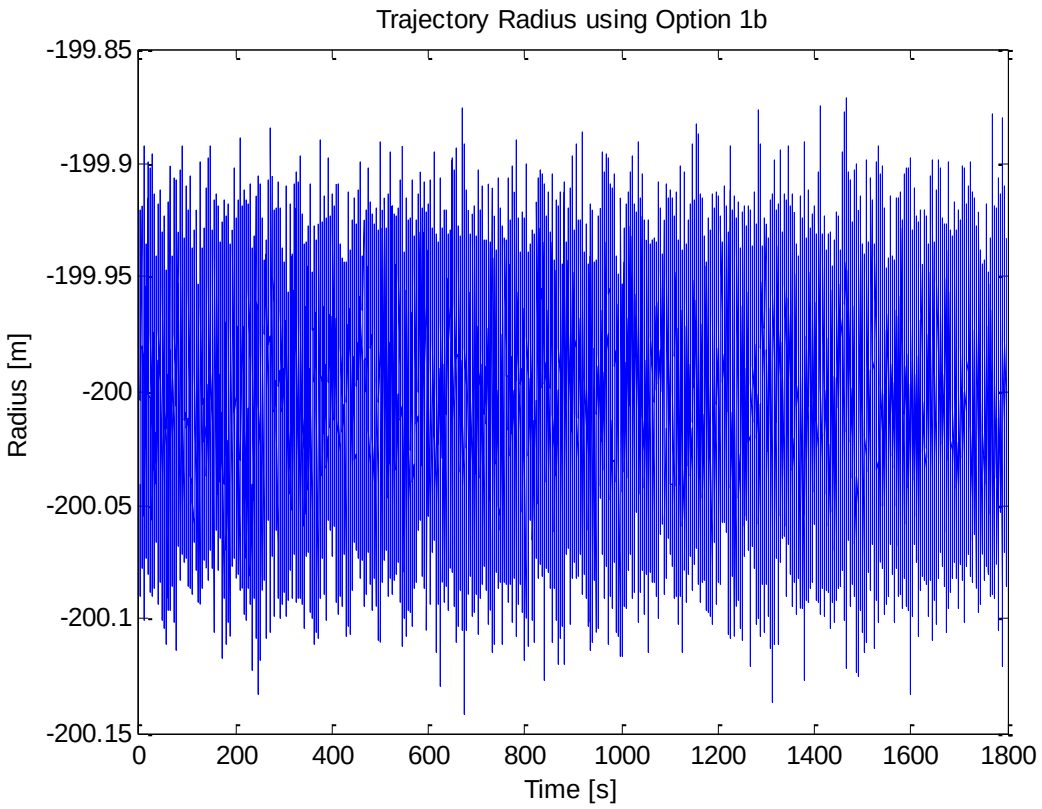

Abb. 15: Estimated radius of the circular track using option 1b

The radius plot of option 2 is shown in Abb. 16 (see chapter A.3.3.3). The average value of the radius is estimated giving a mean value of -199.999 m. The noise of the radius estimation is $\sigma_{\text{Radius,Option2}} = 0.0413\,\text{m}$ which is in the same magnitude as option 1b.

Copyright © 2013, TEGA Konsortium. Alle Rechte vorbehalten.

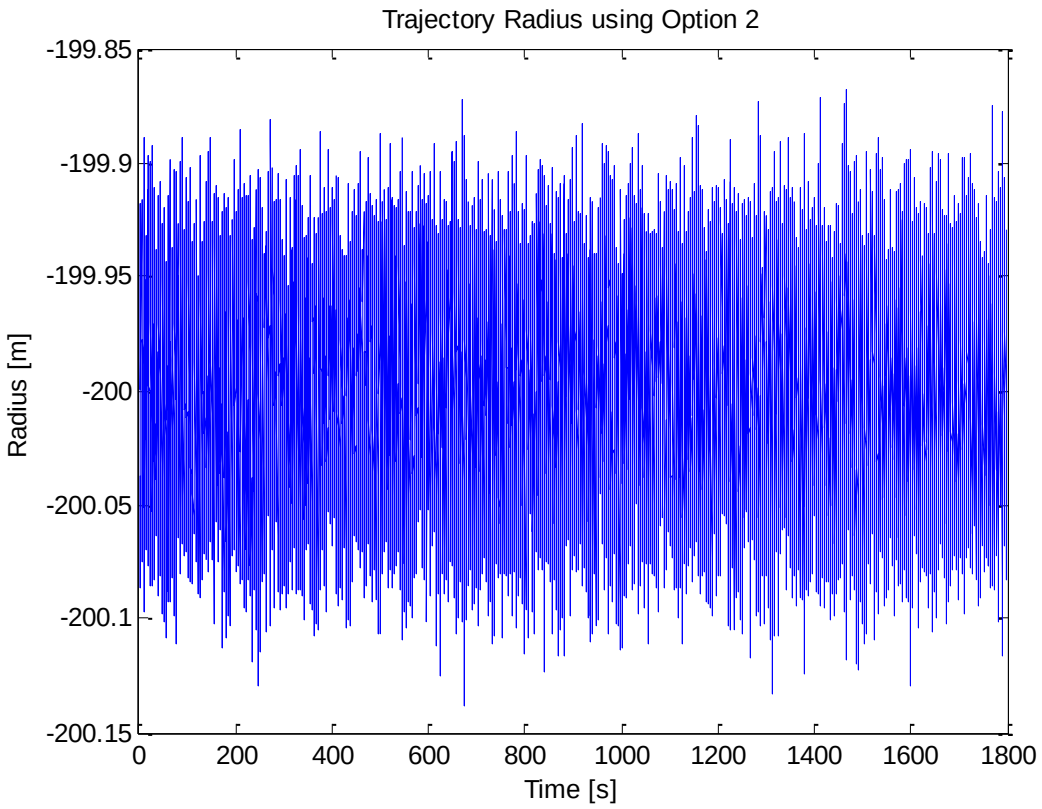

Abb. 16: Estimated radius of the circular track using option 2

A.5.2 Velocity and Wheel Speeds

Having calculated the curvature and yaw rate of the vehicle, the speed of the vehicles reference point and the speed at each of the four wheels can be calculated. It is assumed that the vehicle has the following geometric properties. They are in the magnitude of a typical mid-size sedan:

$$l = 2.705\,\mathrm{m}$$
$$\varepsilon = 0.775\,\mathrm{m} \qquad \textbf{(6-38)}$$

Copyright © 2013, TEGA Konsortium. Alle Rechte vorbehalten.

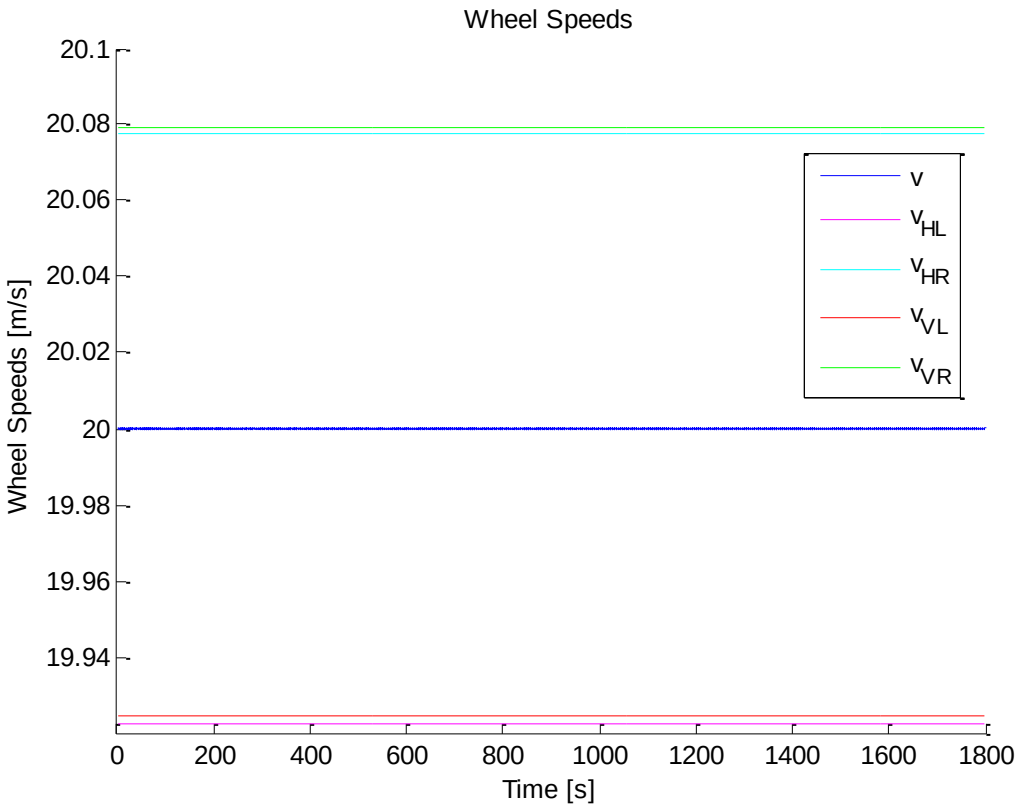

Abb. 17: Velocity of vehicle reference point and all wheels over time

The plot of the velocities over time is shown in Abb. 16. For a uniform circular motion the velocities of the vehicle's reference point and all four wheels is obviously constant. It can be observed that the inner left wheel is spinning at a reduced speed and the outer right wheel is spinning slightly faster than the vehicle's reference point. This is in accordance with the theory. Additionally, the front wheels are also spinning slightly faster than the rear wheel as a result of the slightly enlarged track radius from the wheel base (see Abb. 5).

Abb. 17 shows the corresponding steering angles over time. The effects of the track width can also be observed in this plot. The outer right wheel moves with a larger radius, thus resulting in a smaller steering angle compared to the inner wheel.

Copyright © 2013, TEGA Konsortium. Alle Rechte vorbehalten.

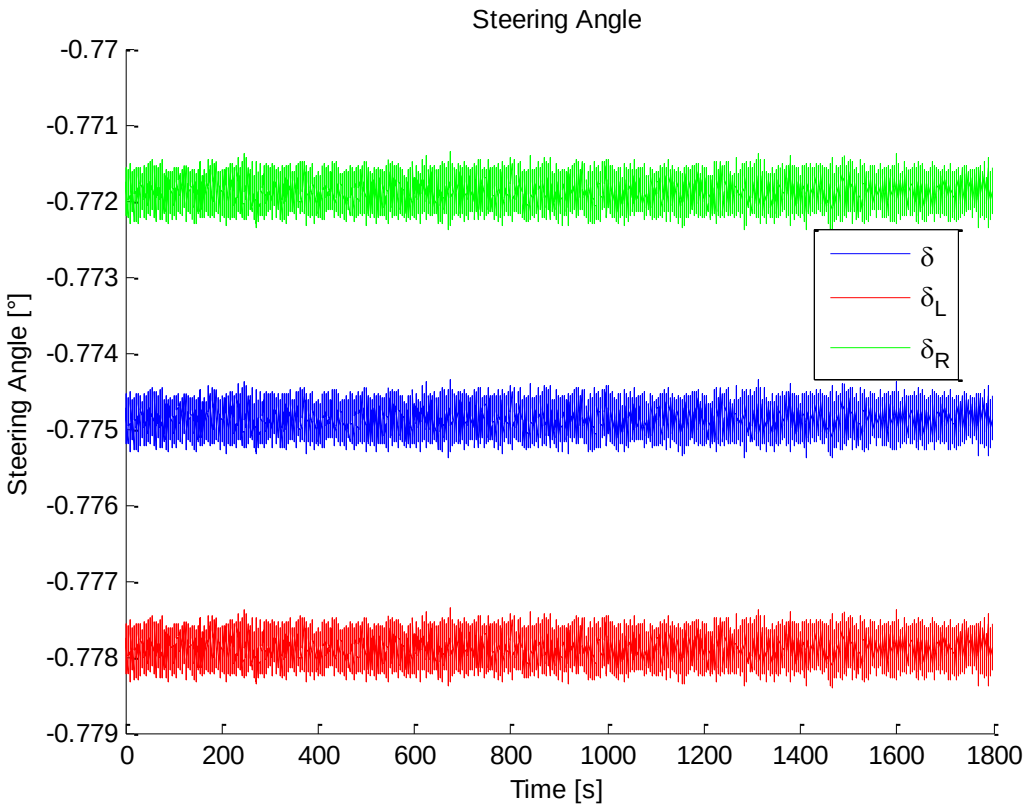

Abb. 18: Steering angle over time

Copyright © 2013, TEGA Konsortium. Alle Rechte vorbehalten.

B TN6: Test Report ‚Fahrzeugdynamik'

B.1 Introduction

B.1.1 Scope of the Document

This document covers the results of the TEGA AP 3500 "Experimentelle Validierung ‚Fahrzeugdynamik'". This document presents the test results of the vehicle data simulation implemented during the project.

Copyright © 2013, TEGA Konsortium. Alle Rechte vorbehalten.

B.2 Methodology

B.2.1 Introduction

The purpose of this document is to ensure that the correct functionality of the developed system is proven under certain test conditions. These test conditions, the corresponding test scenarios and the test results are the main integral parts of this document.

The following paragraphs describe the methodology of the experimental validation of the TEGA vehicle dynamic simulation. The methodology is presented and the corresponding performance indicators are introduced.

B.2.2 Evaluation Strategy

As stated in the project plan, one of the central aims of the project is to provide a simulation facility that allows the simultaneous generation of GNSS RF signals and vehicle sensor data. Therefore it is feasible to compare real life measurement data with simulated vehicle data for a given set of reference trajectories. This methodology requires two separate hardware setups. A test vehicle needs to be equipped with measurement equipment allowing capturing both the reference trajectory and the sensor measurements. Furthermore, a laboratory setup is required that then generates the simulated GNSS signal and the vehicle measurements derived from the reference trajectory. The respective sensor data sets can then be compared to one another.

B.2.3 Experimental Setup

The following sections describe the experimental setups in the research vehicle and under laboratory conditions. The Institute of Flight Guidance operates a Volkswagen Passat Station wagon that can be equipped with the necessary data acquisition devices. Additionally, a full constellation GNSS simulator developed by IFEN is available in the institutes GNSS laboratory. Within the project the simulator was extended to synchronously generate vehicle sensor measurements.

B.2.3.1 Test Drive Hardware Setup

Modern vehicles are equipped with several different kinds of sensors for very different purposes. Typically these sensors are networked thus the usage of the sensor data is not limited to a specific Electronic Control Unit or a specific application. Instead the data is accessible by any bus participant. For research purposes the CAN Bus containing the messages concerning the vehicles movement is mirrored and available via an interface.

The Volkswagen Passat station wagon is used to generate the reference trajectory and collect the corresponding sensor data. The test vehicle is customized by adding an additional

Copyright © 2013, TEGA Konsortium. Alle Rechte vorbehalten.

alternator to meet the power requirements of the measurement and processing hardware. The relevant sensors for example include the odometers of all four wheels.

Abb. 19: Research Vehicle

To reference the dynamic trajectory a GPS / INS system is used. For the calculation of the reference an RTK method is applied. The expected accuracy is in the sub-decimeter range. In challenging environments (e.g. urban or rural scenarios), the accuracy of the reference system deteriorates. The reference is calculated in post-process using a "non-causal" calculation tool. A combined forward-backward calculation is applied. Within the project the software “Inertial Explorer” from NovAtel is used.

The vehicle sensor data is streamed via CAN to an automotive PC from Spectra. It is equipped with an Intel quad core CPU, 8 GB RAM, a Vector PCI CAN device and 256 GB SATA solid state disk allowing up to 195 MB/s writing speed. For research in the field of vehicle state estimation the Institute of Flight Guidance utilizes the “Automotive Data and Time-Triggered Framework” (ADTF). The software is commonly used in the automotive industry for the development of advanced driver assistance systems. A central component of

Copyright © 2013, TEGA Konsortium. Alle Rechte vorbehalten.

the framework is the ability to record and play back measurement data. A Time Master developed by the IFF is used to time stamp the CAN data messages.

Within ADTF the systems are assembled from modules. Standard modules such as the connection of common hardware are provided with the framework. Custom modules can be implemented in C++ by the user. Every module is implemented as a dynamic library (DLL) and interpreted by the framework. During past projects related to vehicle navigation the Institute of Flight Guidance has developed an exhaustive set of ADTF modules for data acquisition and processing.

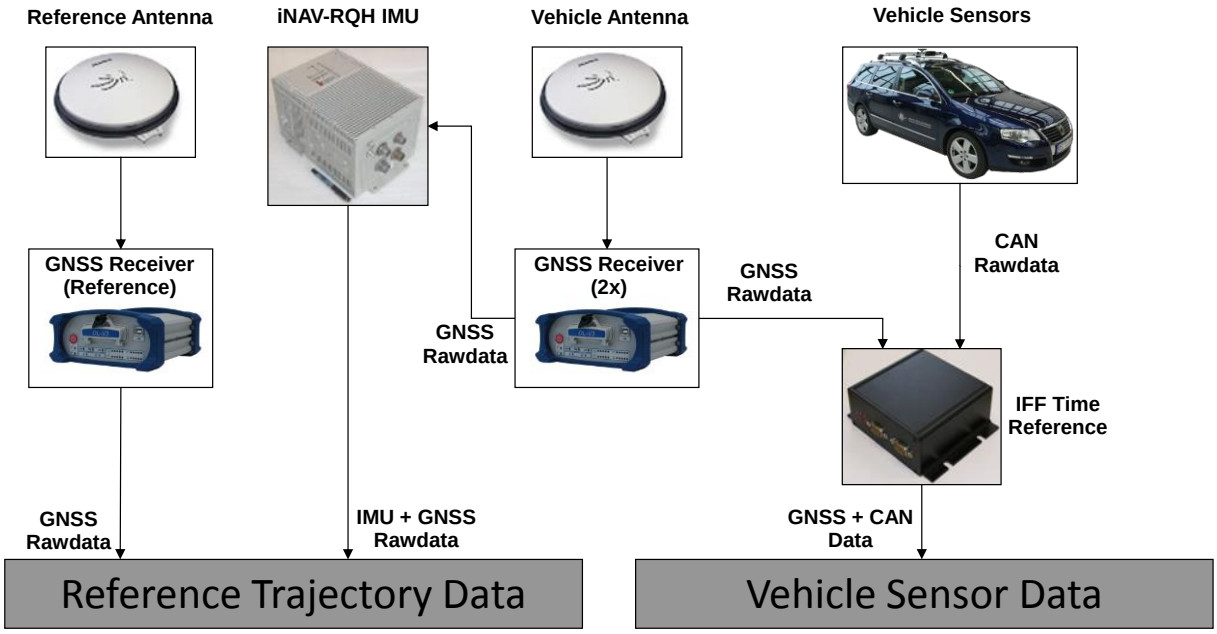

Abb. 20: Schematic Data Acquisition Setup

B.2.3.2 Laboratory Hardware Setup

The heart of the experimental test setup in the laboratory is a full constellation simulator developed by IFEN. It is able to simulate a constellation of GPS and Galileo satellites. Simulated GNSS signals are available at an RF output. Depending on the constellation and the motion of the antenna the travel times of the signals and the corresponding Doppler shifts are simulated.

As part of the TEGA project the constellation simulator is extended by the functionality to emulate data from typical vehicle dynamics sensors synchronously and output them via a

Copyright © 2013, TEGA Konsortium. Alle Rechte vorbehalten.

CAN interface. The parameters of the model vehicle can be adapted so that a realistic emulation of the test vehicle of the Institute possible.

The GNSS Signal is processed using a commercial GNSS Receiver integrated in the IFF Time Master. The vehicle sensor measurements are captured using a USB CAN device from "Vector". The setup is very similar to the setup used for the test drives. The measurements are time stamped by the Time Master.

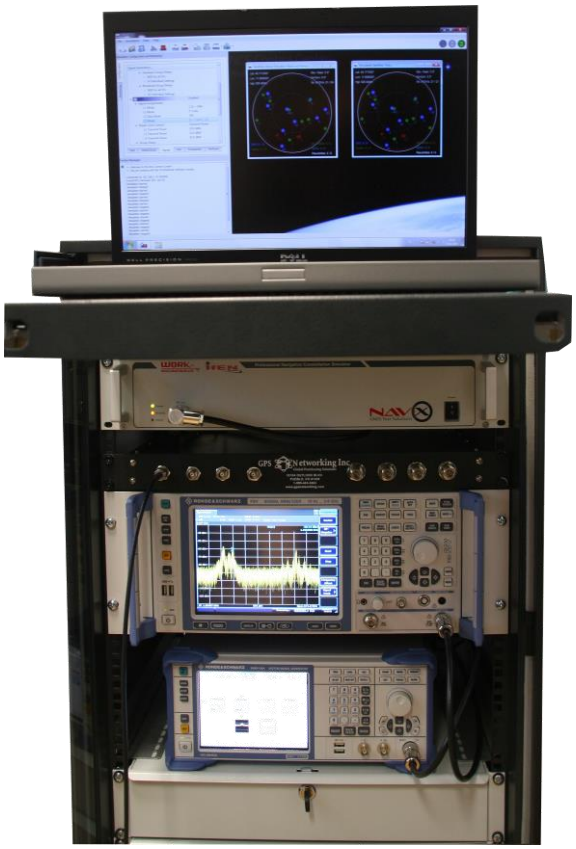

Abb. 21: GNSS Constellation Simulator

B.2.4 Analysis Script

The analysis of the gathered data is conducted in post process using an analysis tool written in Matlab. The evaluation logic follows the demands described in Chapters B.2.2 and B.2.3. The evaluation process is illustrated in Abb. 22.

Copyright © 2013, TEGA Konsortium. Alle Rechte vorbehalten.

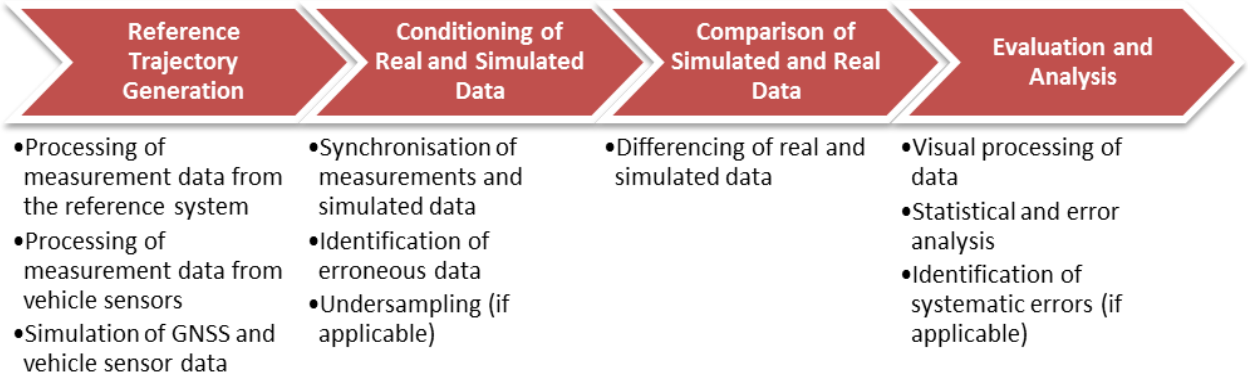

Abb. 22: Comparison of real life and simulated vehicle sensor data

Firstly, the recorded data from the reference system and the vehicle sensor data are preprocessed. The reference trajectory is generated using “Inertial Explorer” from Novatel. The calculated trajectory is exported as a CSV file for further processing. Besides the GPS time stamps the position and velocity are exported in ECEF coordinates. The format is chosen in a way that allows the direct import of the trajectory into the control center software of the GNSS constellation simulator.

Copyright © 2013, TEGA Konsortium. Alle Rechte vorbehalten.

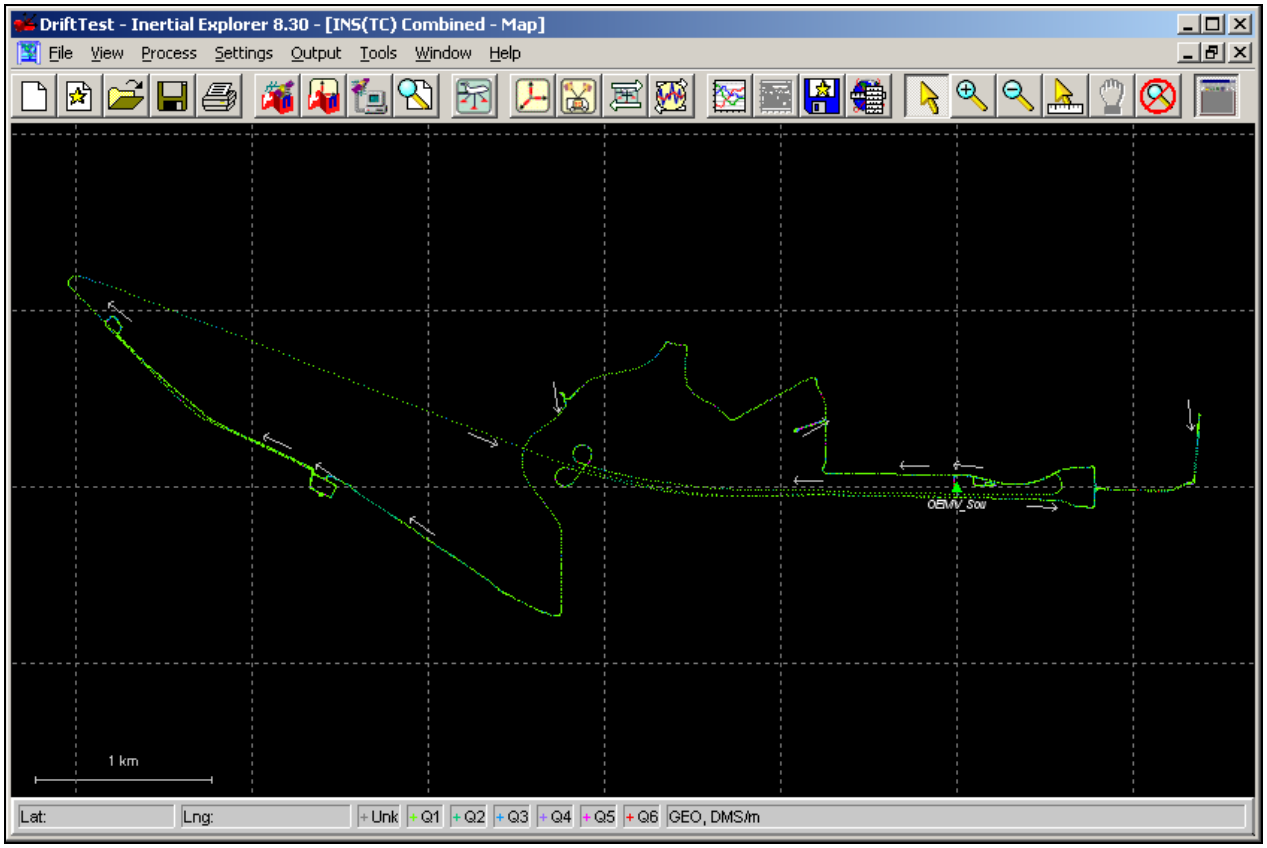

Abb. 23: Reference trajectory generation

Corresponding to the vehicle's position and velocity a second data set containing the sensor measurements is recorded. It is processed in ADTF. The data in this set is also GPS time stamped so that the sensor measurements can be allocated to the corresponding position and velocity values. The data is also exported as a CSV file for further processing in Matlab.

Based on the reference trajectory the GNSS simulator is able to generate a data set of emulated vehicle sensor data. The data are recorded and processed using a setup similar to the data acquisition during the test drives.

When all data are available, real life measurements and simulated data need to be conditioned. The vehicle sensors and the GNSS simulator are unlikely to have the exact same sampling intervals concerning the CAN data. Thus, an interpolation and resampling of the data is feasible. Additionally, the recorded data from the test drive may suffer from outages or outlier measurements that need to be removed.

Copyright © 2013, TEGA Konsortium. Alle Rechte vorbehalten.

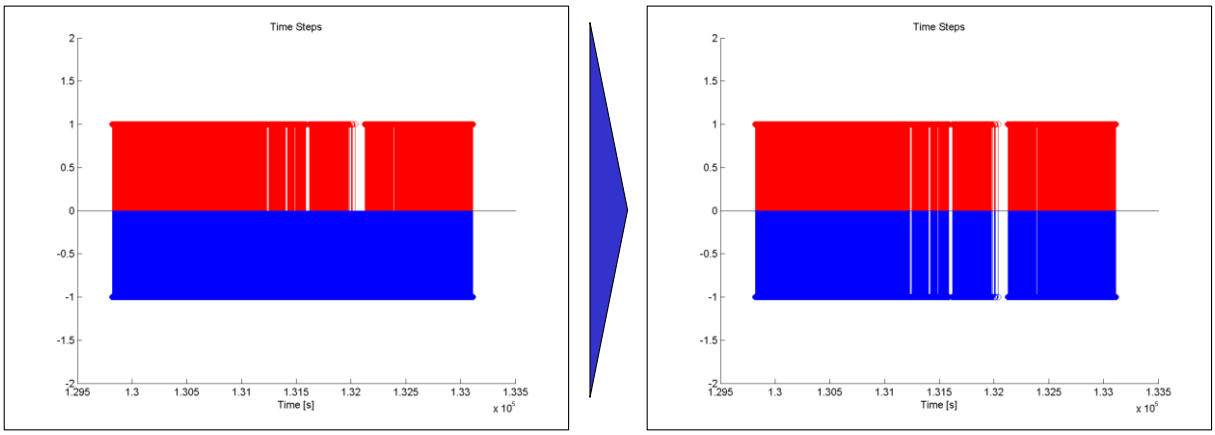

Abb. 24: Conditioning of real life and simulated vehicle measurements

When the data samples are aligned and matched to each other the core part of the evaluation script is executed. This part especially includes all comparison and differencing of real life and simulated data.

Copyright © 2013, TEGA Konsortium. Alle Rechte vorbehalten.

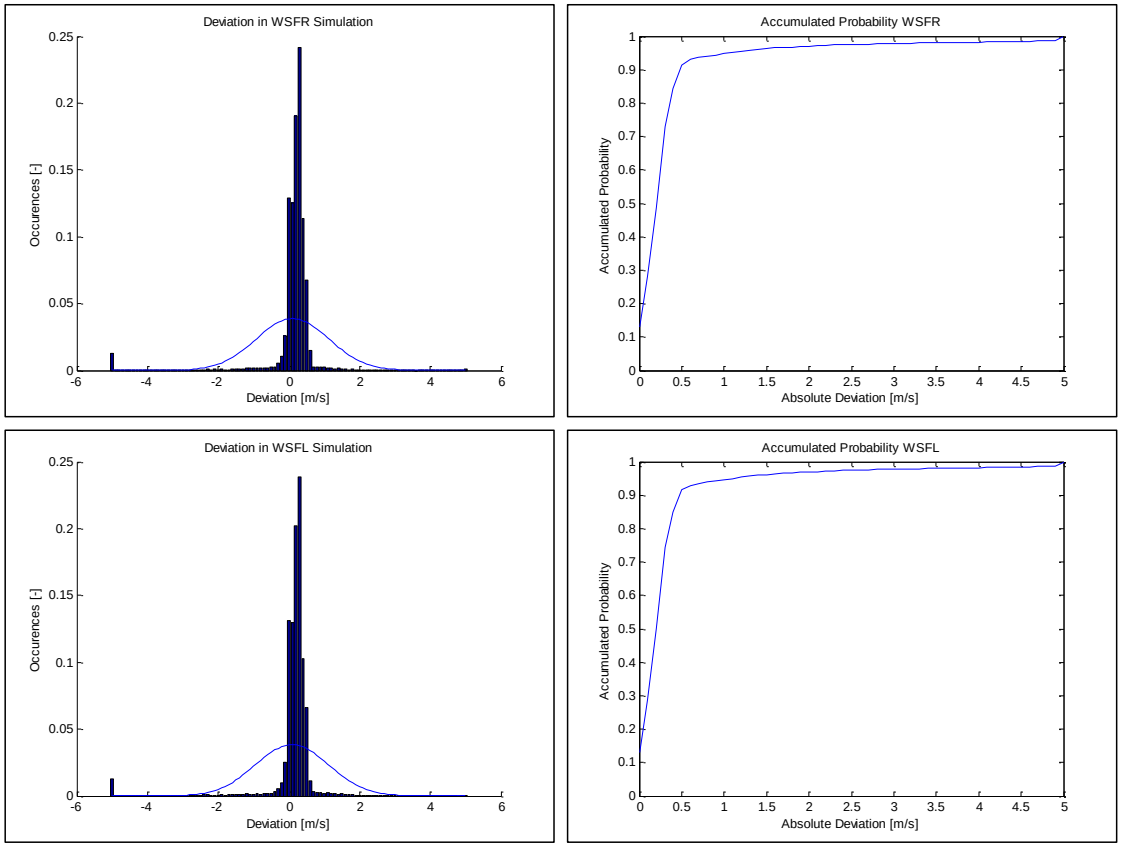

Abb. 25: Deviation analysis of real life and simulated vehicle sensor data

The evaluation process then consists of the comparison of the simulated and real life vehicle sensor measurements at every time stamp both values exist. The differences between them are evaluated, e.g. concerning scattering or systematic offsets.

Copyright © 2013, TEGA Konsortium. Alle Rechte vorbehalten.

B.3 Test Drive Scenarios

In the validation phase of the project, several test drives have been carried out in the region of Braunschweig. Different environments such as rural roads and highways have been chosen for evaluation.

B.3.1 Highway Scenario

A highway scenario has been chosen for the evaluation of the vehicle sensor simulation system. The trajectory plot is shown in Abb. 26. The origin of the trajectory is the Institute of Flight guidance south of the research airport of Braunschweig. The trajectory has been chosen so that motion in all four cardinal directions is granted.

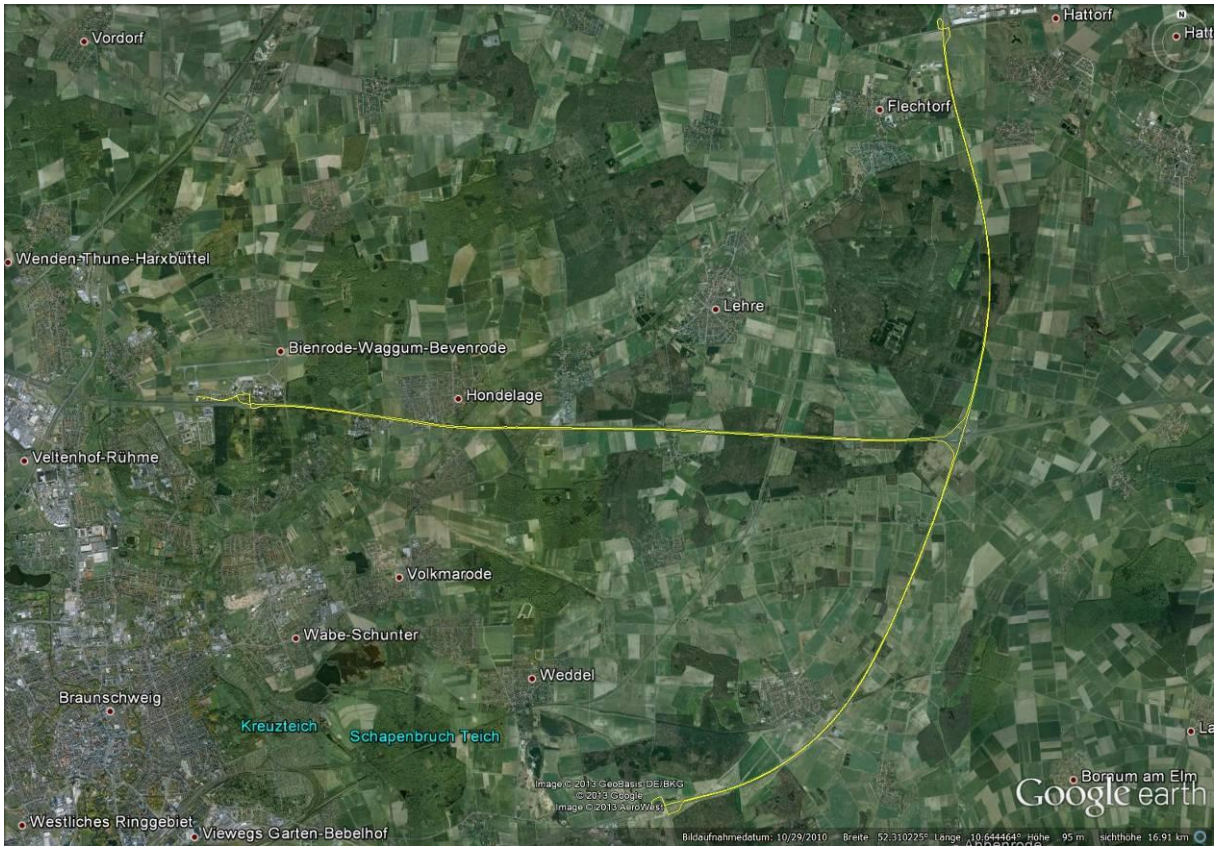

Abb. 26: Trajectory of the highway scenario

After entering the highway east of the institute, the trajectory heads eastwards for about 12 km until a highway junction is reached. The highway is left continuing north for about 7 km. After leaving the highway and turning in the opposite direction the highway is followed south

Copyright © 2013, TEGA Konsortium. Alle Rechte vorbehalten.

for about 15 km. Again the direction is changed and a northwards passage of 8 km follows until reaching the highway junction again. Turning back west towards the institute another passage of 12 km finishes this scenario.

The travel speeds are within the typical range for German highways. A plot of the vehicle's speed is presented in Abb. 27.

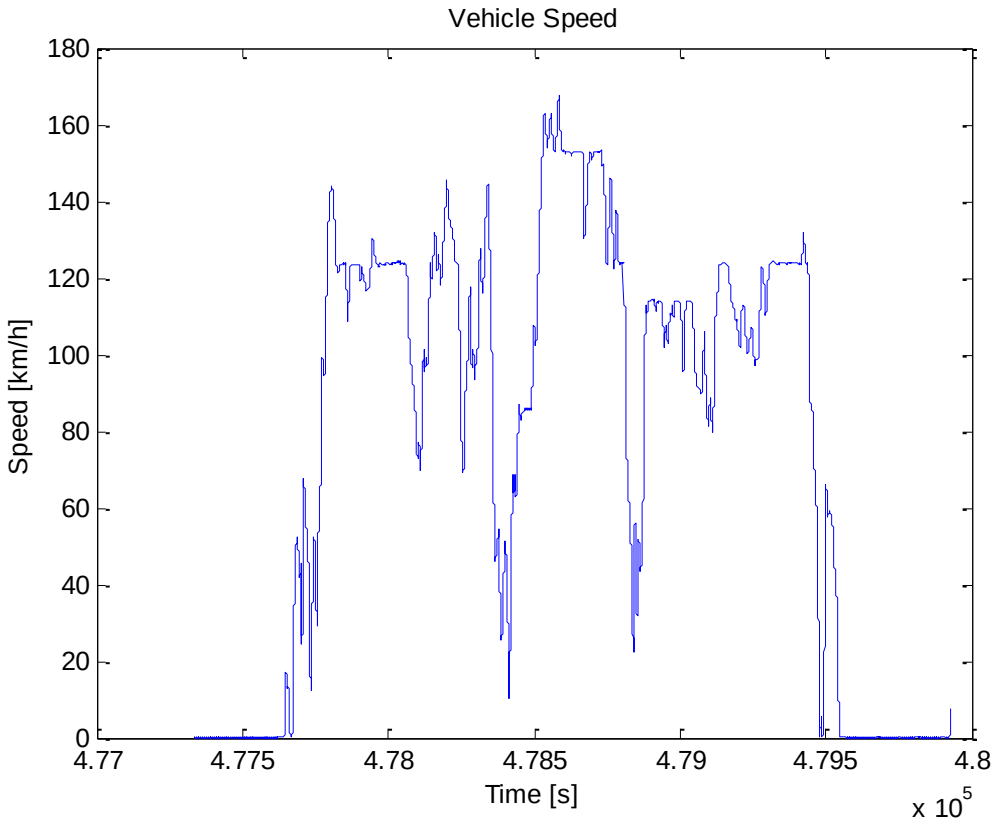

Abb. 27: Vehicle speed over time in the highway scenario

The diagram shows that after entering the highway typically a speed between 80 km/h and 160 km/h is maintained, disregarding the times when the highway is left or entered.

Corresponding to the vehicle speed the following Abb. 28 shows the vehicle's heading over time. The main directions of travel of the five parts of the test drive can be observed in that diagram. After entering the highway a heading of ~90° is maintained. Following that part the heading increases from ~190° until it reaches ~270°. A sector in the northern direction follows until the vehicle is heading back west with about 270°.

Copyright © 2013, TEGA Konsortium. Alle Rechte vorbehalten.

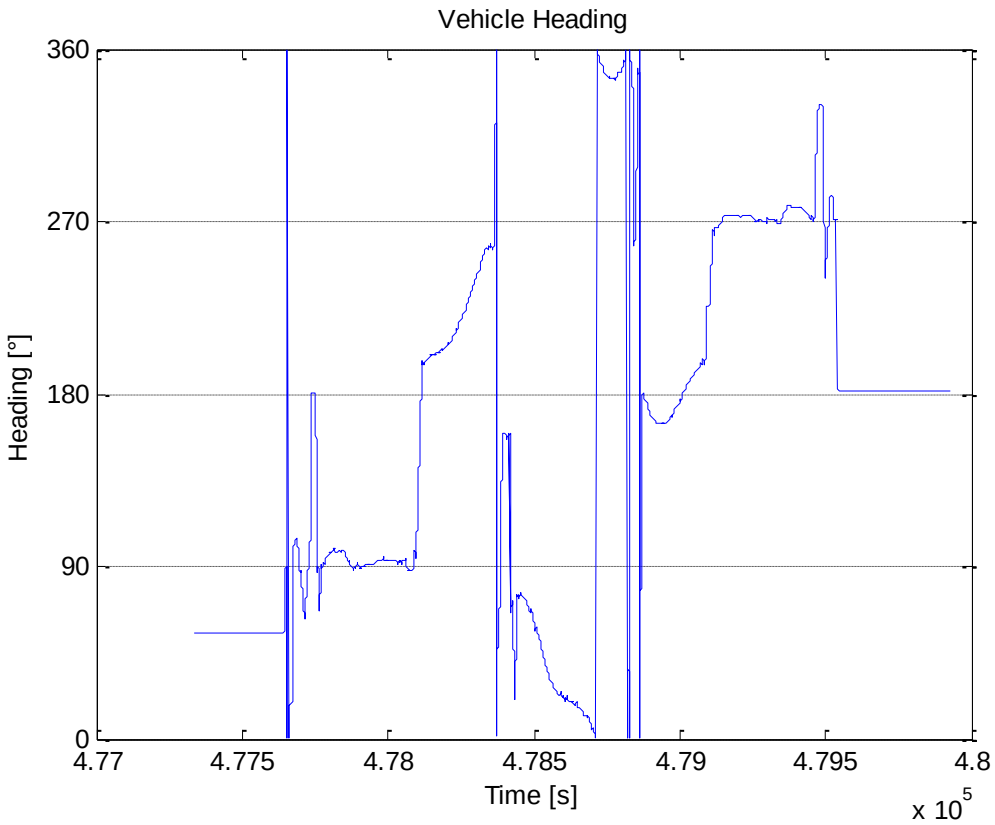

Abb. 28: Vehicle heading over time in the highway scenario

B.3.2 Combined Highway/Urban/Rural Scenario

Additionally to the highway scenario combined highway/urban/rural test drives have been evaluated, as they are more demanding towards the vehicle sensor data generation. The trajectory plot is shown in Abb. 29. The test drive is started east of the research airport of Braunschweig. After the reference system is initialized, the highway A2 Braunschweig–Berlin is driven eastwards for 12 km followed by the return path until again reaching the research airport.

After leaving the highway a rural road is taken eastwards around the surrounding towns of Braunschweig. After returning to Braunschweig, rural roads are driven for about 30 km north of Braunschweig. The rural section is then followed by an urban part of the scenario. Approximately 15 km are driven on the streets of Braunschweig, mainly in the eastern residential zones. The scenario is finished driving approximately another 25 km on highways south and west of Braunschweig.

Copyright © 2013, TEGA Konsortium. Alle Rechte vorbehalten.

Abb. 29: Trajectory of the combined highway/urban/rural scenario

The velocity over time of the vehicle during the test drive is presented in Abb. 30. In the first part of the plot, typical highway speeds up to ~170 km/h can be observed. After leaving the highway, a section in suburban and rural conditions is driven. Velocities in the suburban regions rarely exceed 50 km/h, in the rural regions velocities up to 100 km/h can be observed.

The following period in urban conditions again shows the typical velocities driven in city centers. Frequent stopping and average velocities of ~30 km/h are observable. The final section on the highway heading back to the institute again bears the highway velocities of the magnitude of ~100 km/h.

Copyright © 2013, TEGA Konsortium. Alle Rechte vorbehalten.

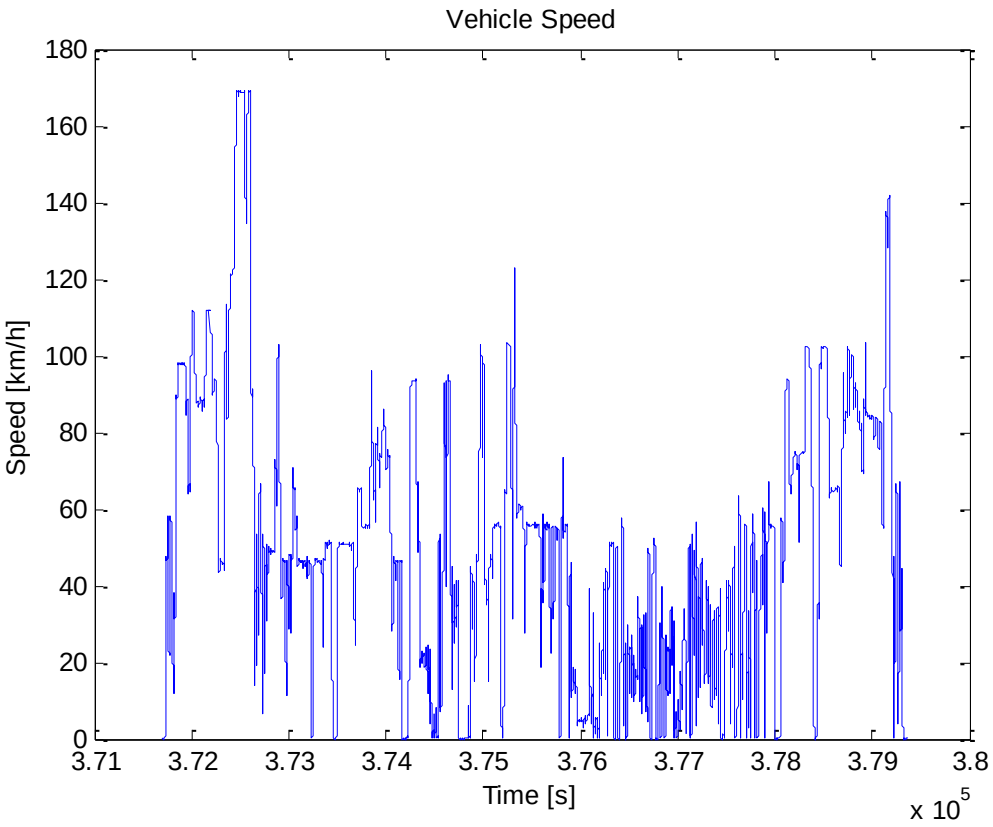

Abb. 30: Vehicle speed over time in the combined highway/urban/rural scenario

In addition to the vehicle speed, the vehicle's heading over time is shown in Abb. 31. In the first highway section, main directions of travel in eastern and western direction can be observed. The second section through the suburban areas of Braunschweig also mainly shows eastern and western travel directions.

The following rural and urban sections of the scenario show a variable heading. No main travel directions are observable. The final part of the scenario driven on the highway towards the research airport again shows a northeastern travel direction.

Copyright © 2013, TEGA Konsortium. Alle Rechte vorbehalten.

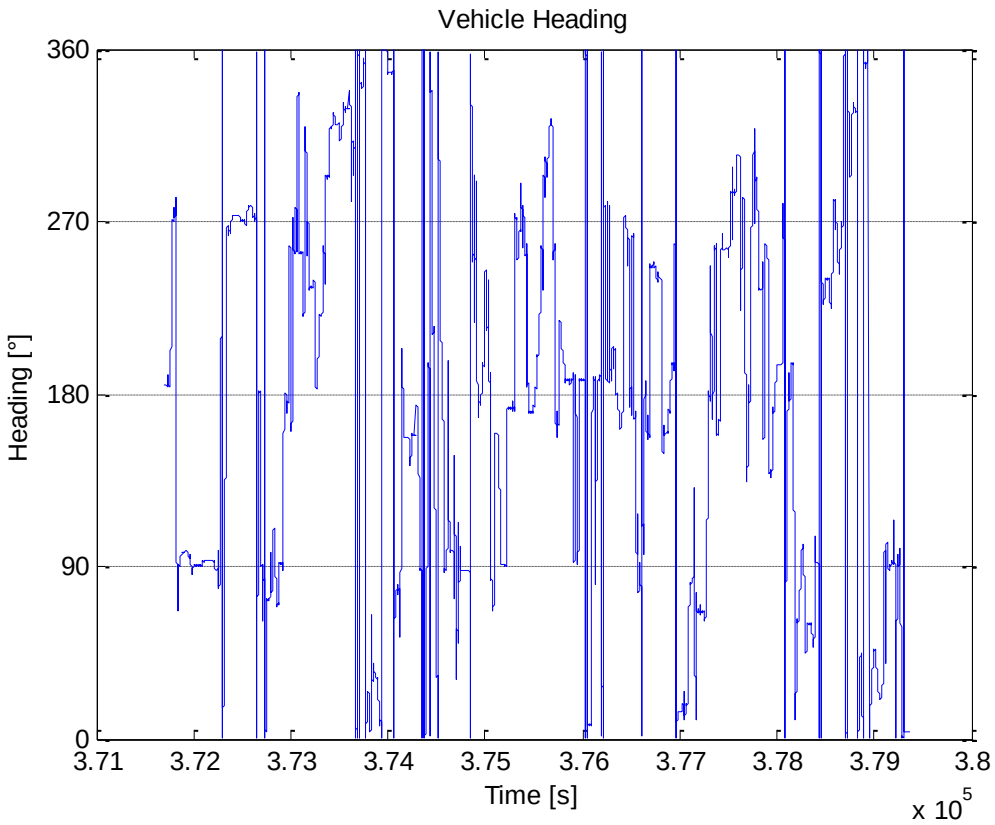

Abb. 31: Vehicle heading over time in the combined highway/urban/rural scenario

B.3.3 Urban Scenario

As a third evaluation scenario a track was chosen that focuses on urban traffic. The plot of the trajectory is shown in Abb. 32. The origin of the test drive is east of the research airport of Braunschweig. After the initialization of the reference system the scenario begins driving along the research airport and entering Braunschweig from the north. Braunschweig is then crossed in southern direction in urban traffic situations driving approximately 15 km, including stops in the northern and southern parts of Braunschweig. After crossing the city a short highway section is driven eastwards and back westwards in order to again enter Braunschweig from the southeast.

After entering Braunschweig from the southeast the trajectory crosses the inner city exiting to the east. The track leads through the eastern suburban areas of Braunschweig. In total, approximately 15 km are driven in that area until the research airport is again reached.

Copyright © 2013, TEGA Konsortium. Alle Rechte vorbehalten.

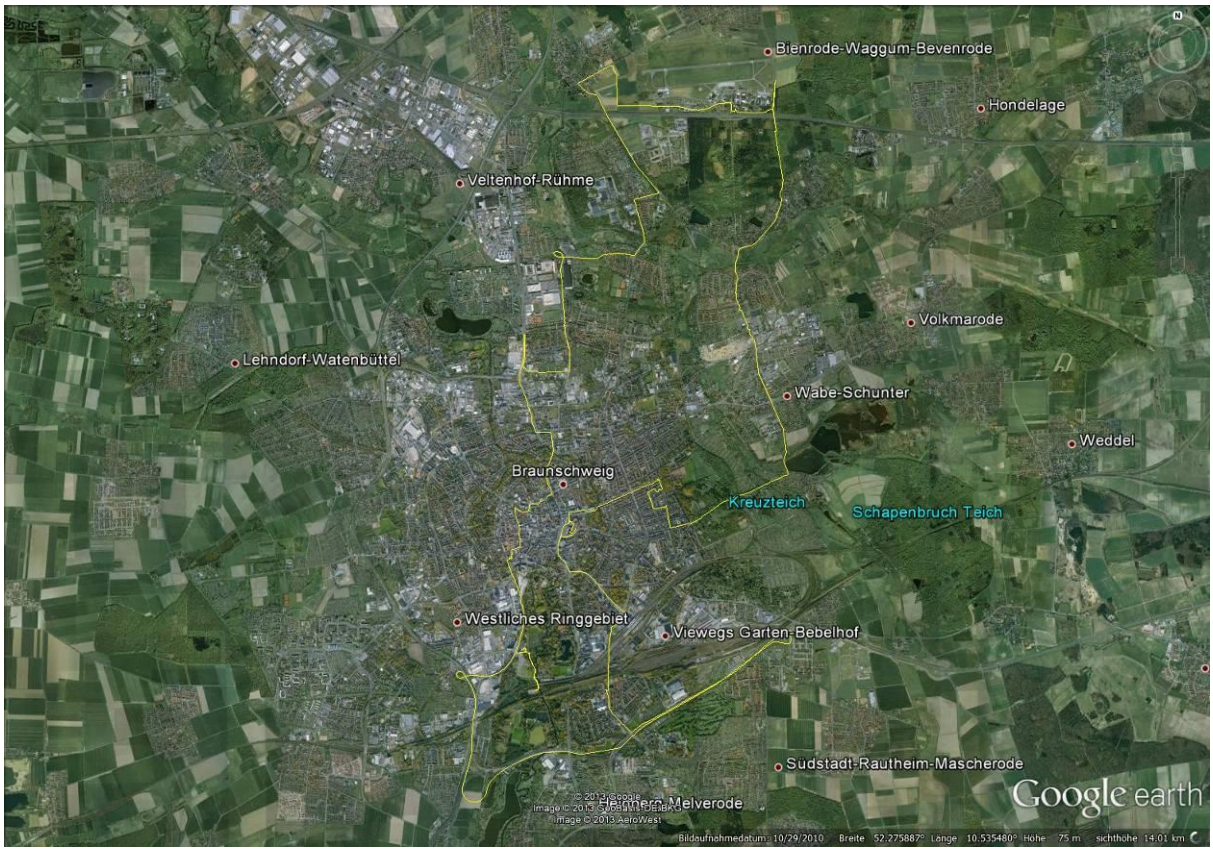

Abb. 32: Trajectory of the urban scenario

The following **Fehler! Verweisquelle konnte nicht gefunden werden.** shows the velocity over time of the vehicle during the test drive in urban conditions. The first sections until the second major stop show typical speeds of urban traffic of about 60 km/h or less including several short stops at intersections.

After the second major stop the increase of the velocity illustrates the highway section of the scenario. The following period then shows the final part of the scenario in urban conditions with typical velocities of less than 60 km/h before the origin of the scenario is reached.

Copyright © 2013, TEGA Konsortium. Alle Rechte vorbehalten.

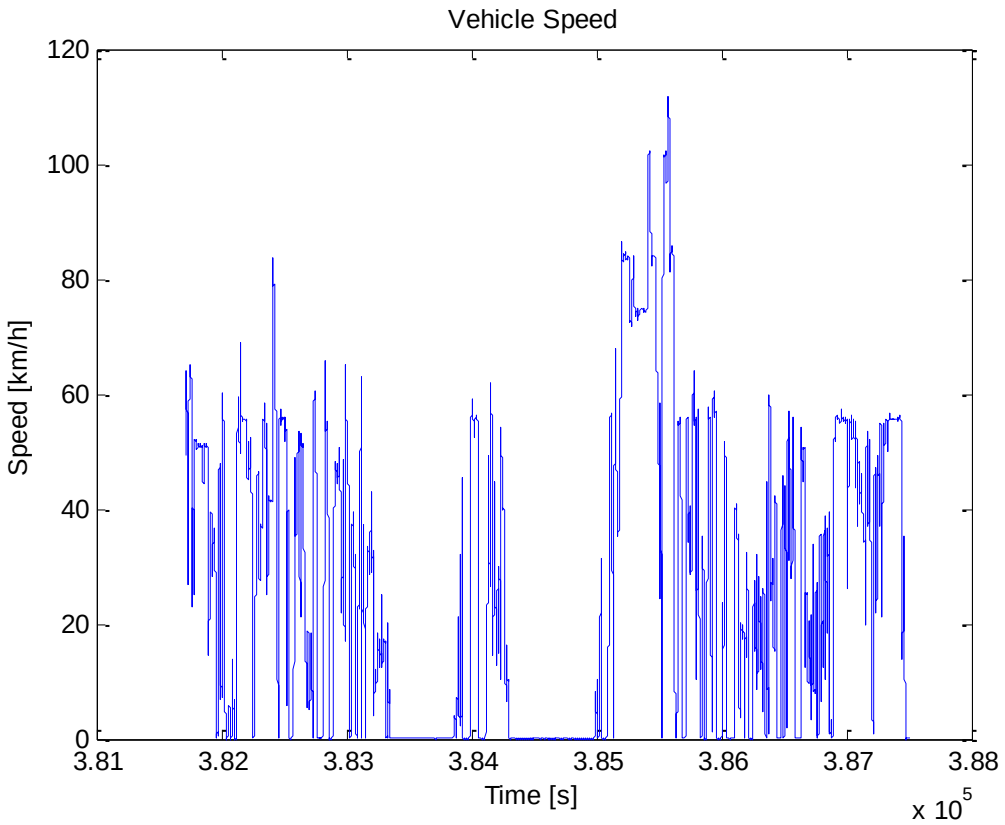

Abb. 33: Vehicle speed over time in the urban scenario

The heading plot over time shown in Abb. 34 initially shows a westbound track followed by a southern passage which represents the initial drive through Brauschweig from north to south. After the second major stop the highway section can be observed, initially eastbound and afterwards westbound.

After again entering Braunschweig, the way back to the research airport in northern direction with shorter eastbound passages can be observed.

Copyright © 2013, TEGA Konsortium. Alle Rechte vorbehalten.

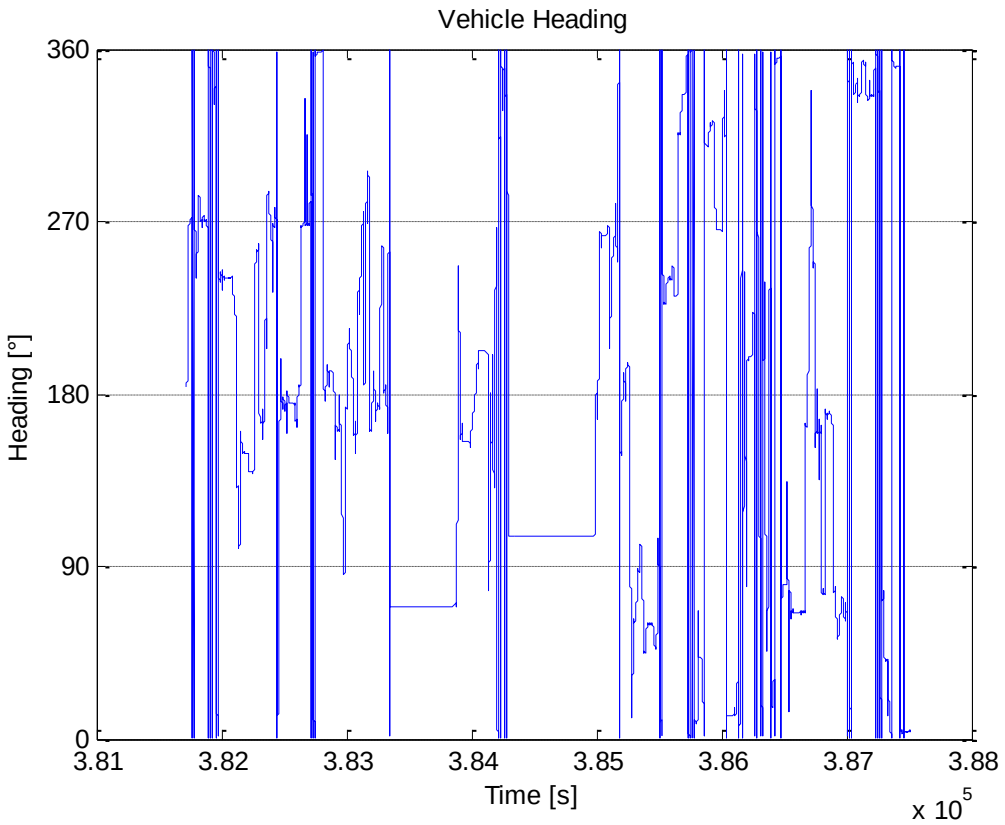

Abb. 34: Vehicle heading over time in the urban scenario

Copyright © 2013, TEGA Konsortium. Alle Rechte vorbehalten.

B.4 Experimental Results

B.4.1 Highway Scenario

The evaluation of the sensor data in the highway scenario indicates positive results. shows the velocity profiles over time of the four wheel speed sensors. The green lines represent the vehicle speed of the measurement data from the research vehicle. The red lines show the simulated vehicle speed over time. In the presented plots the simulated and the real measurement values are virtually congruent. No significant outlier is visible from the plots.

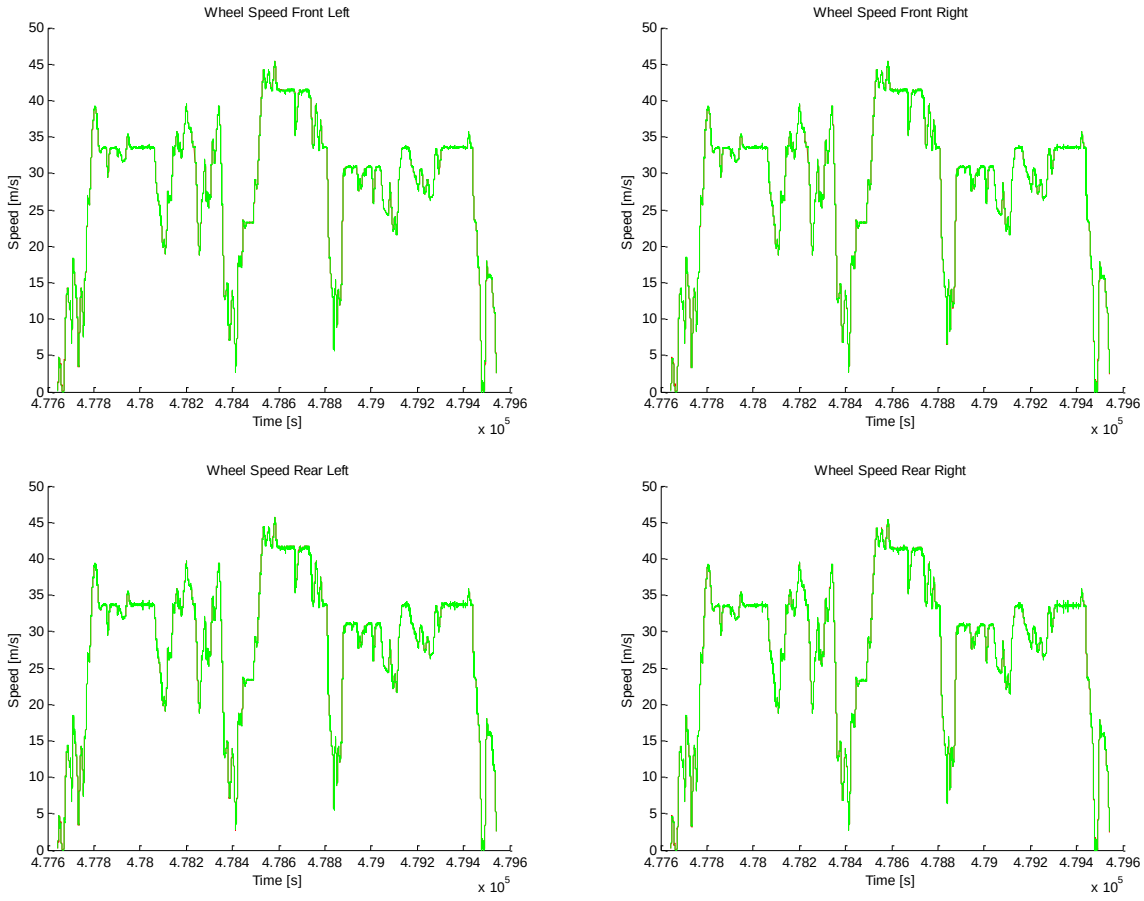

Abb. 35: Plots of real (green) and simulated (red) wheel speeds

In addition to the plots of the velocity over time, the histograms of the difference between simulated and real wheel speed sensor measurements are presented in Abb. 36. It can be

Copyright © 2013, TEGA Konsortium. Alle Rechte vorbehalten.

observed that no measurements exist with an offset larger than 1 m/s. The histograms clearly show a mean value close to zero with very little scatter.

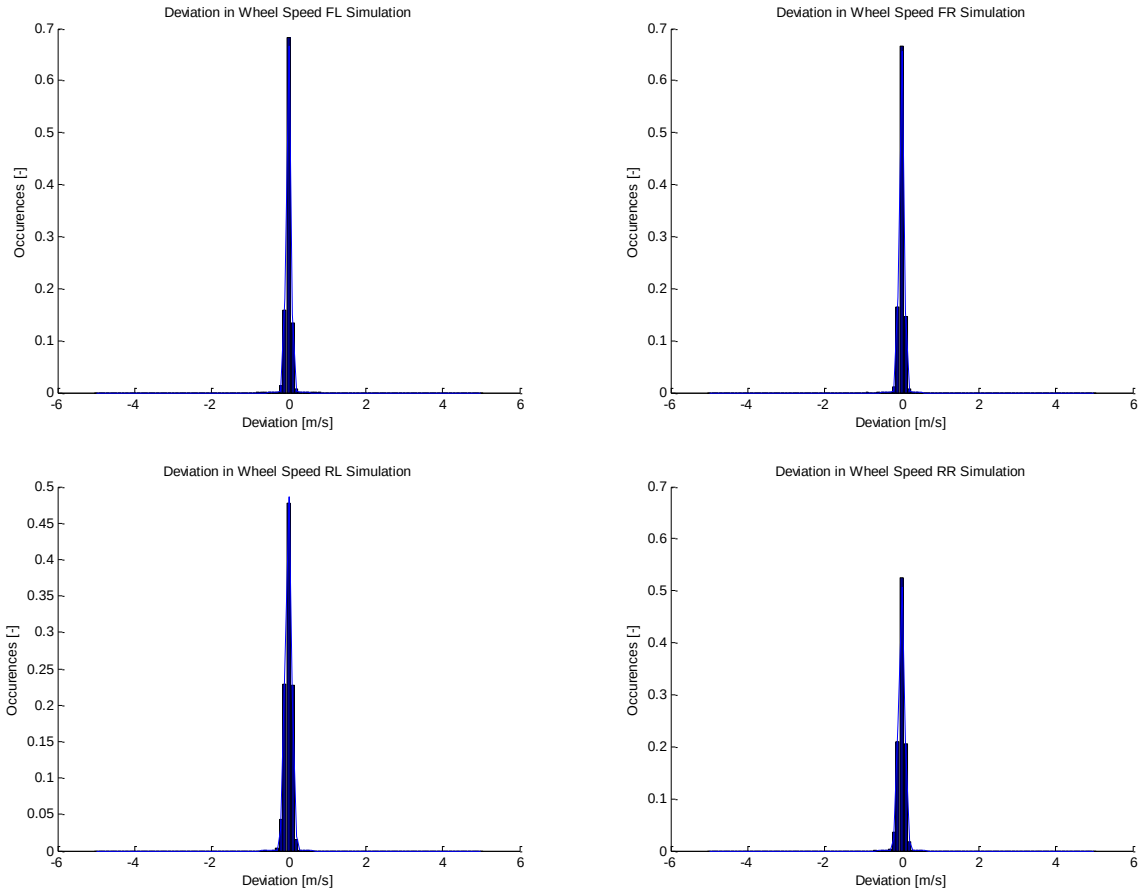

Abb. 36: Histogram plots of the deviation in the wheel speeds

The corresponding mean values and standard deviation are shown in Tab. 4. The mean offsets between simulated and real measurement values are in the order of 10^{-3} m/s. The respective values of the standard deviation are in the order of 10^{-2} m/s. Values in this order of magnitude can also result from noise and measurement errors of the research vehicle. It can be stated, that the simulation of wheel speed sensor measurements in this scenario is reasonable.

Tab. 4 Mean values and standard deviation of the offsets between simulated and real wheel speeds

Wheel	*Mean Offset [m/s]*	*Standard Deviation [m/s]*
Front Left	-0.0034	0.0598

Copyright © 2013, TEGA Konsortium. Alle Rechte vorbehalten.

Front Right	-0.0029	0.0607
Rear Left	-0.0064	0.0818
Rear Right	-0.0046	0.0785

The plots of the accumulated probability of the deviation are presented in Abb. 37. All wheel speed sensors show a similar behavior. More than 90% of the simulated measurements have an offset of 0.1 m/s or less from the measurement data captured from the research vehicle.

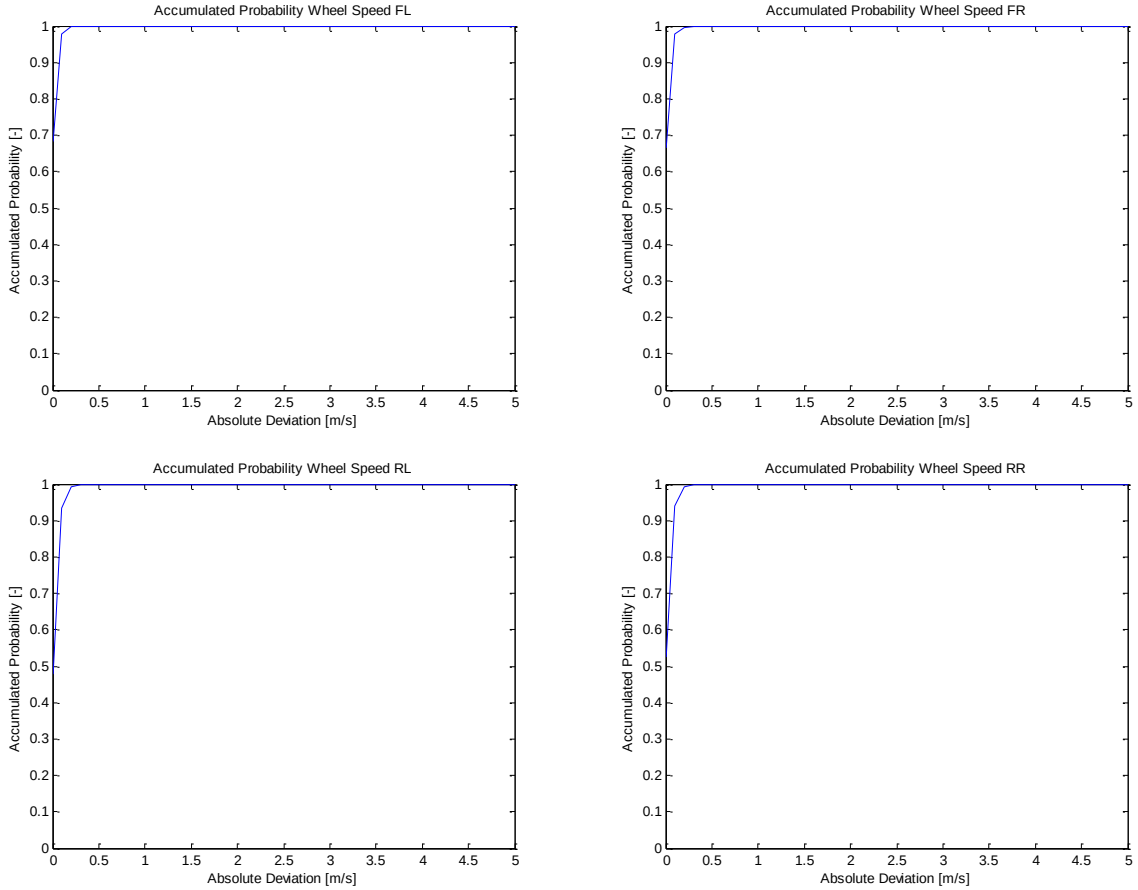

Abb. 37: Accumulated probability of the wheel speed deviation

B.4.2 Combined Highway/Urban/Rural Scenario

The evaluation of the sensor data in the combined highway/urban/rural scenario shows similar results to the highway scenario. Abb. 38 shows the corresponding velocity profiles over time of the wheel speed sensors. Again, the green lines represent the measurement data from and

Copyright © 2013, TEGA Konsortium. Alle Rechte vorbehalten.

the red lines show the simulated vehicle speed data. As in the highway scenario the plots are virtually congruent. Only minor outliers are visible especially at low speeds.

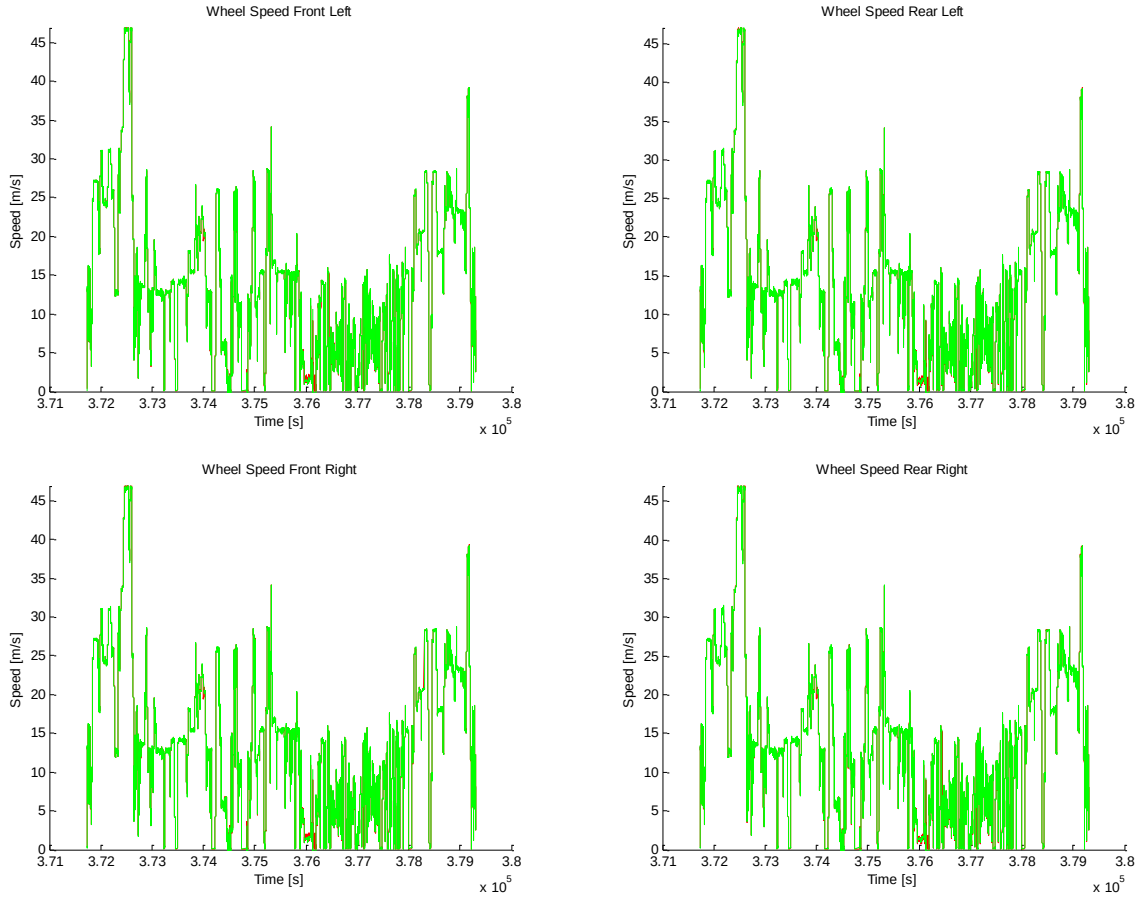

Abb. 38: Plots of real (green) and simulated (red) wheel speeds

The corresponding histograms of the difference between simulated and real wheel speed sensor measurements are shown in Abb. 39. Again, virtually no measurements with an offset larger than 1 m/s are observable. The histograms show a distinct mean value close to zero with hardly any scatter.

Copyright © 2013, TEGA Konsortium. Alle Rechte vorbehalten.

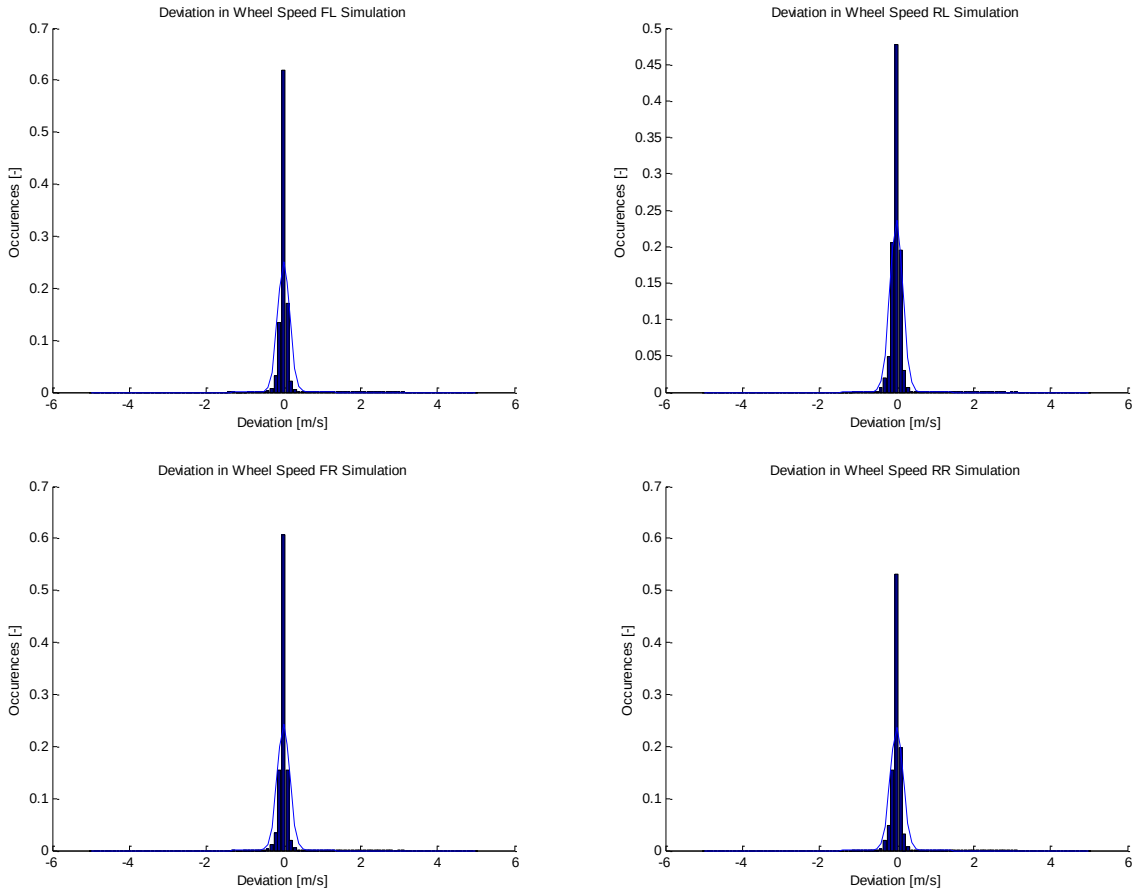

Abb. 39: Histogram plots of the deviation in the wheel speeds

The respective mean values and standard deviation of the offset between measurements and simulation are shown in Tab. 5. The mean offsets are in the order of 10^{-3} m/s which is the same magnitude as the highway scenario. The values of the standard deviation are slightly larger and result in the order of 10^{-1} m/s. As stated earlier, urban scenarios are more demanding towards the measurement data generation. But in accordance to the highway scenario it can be concluded, that the simulation of wheel speed sensor measurements in this scenario is reasonable.

Tab. 5 Mean values and standard deviation of the offsets between simulated and real wheel speeds

Wheel	***Mean Offset [m/s]***	***Standard Deviation [m/s]***
Front Left	0.0076	0.1592

Copyright © 2013, TEGA Konsortium. Alle Rechte vorbehalten.

Front Right	0.0027	0.1645
Rear Left	-0.0030	0.1694
Rear Right	0.0050	0.1687

The corresponding accumulated probability of the deviation is plotted in Abb. 40. Again, the wheel speed sensors show a consistent behavior. More than 90% of the simulated measurements have an offset of 0.2 m/s or less from the measurement data captured from the research vehicle.

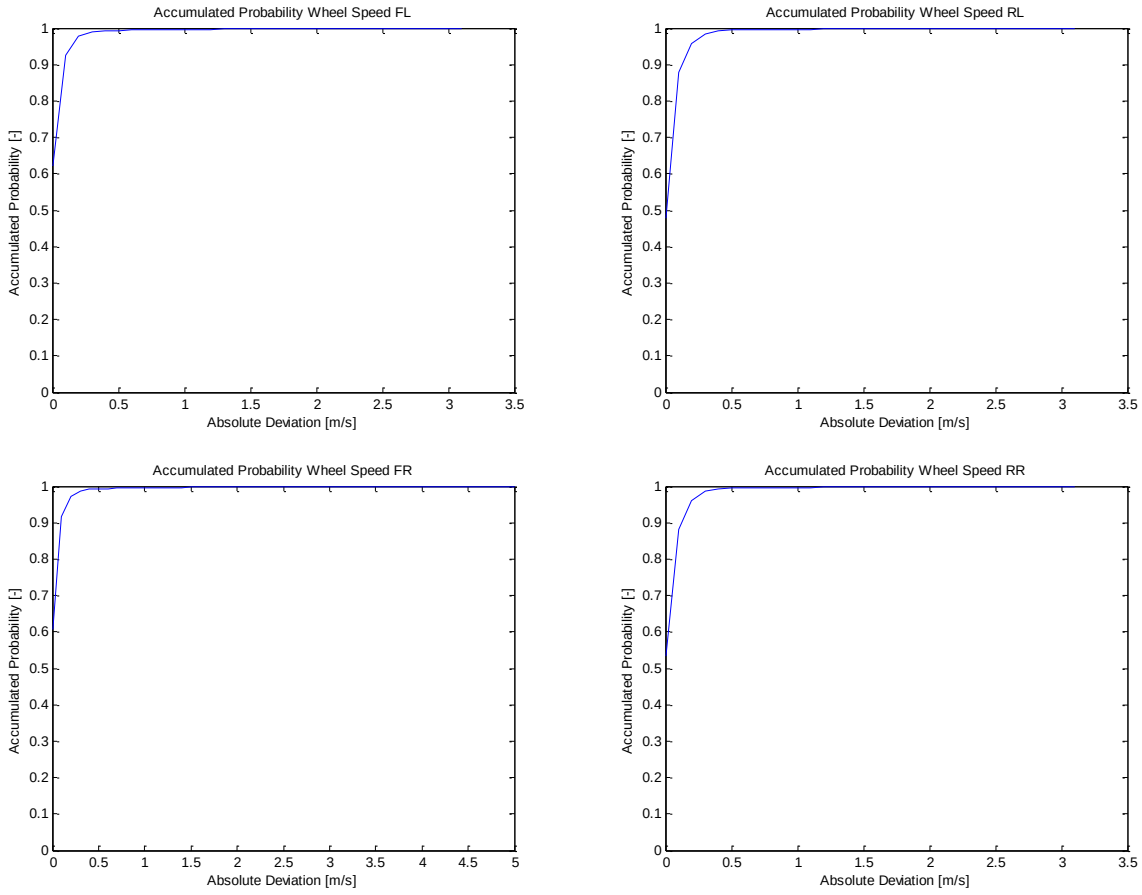

Abb. 40: Accumulated probability of the wheel speed deviation

Copyright © 2013, TEGA Konsortium. Alle Rechte vorbehalten.

B.4.3 Urban Scenario

The results of the evaluation of the sensor data in the urban scenario confirm the impression from the previous scenarios. In Abb. 41 the velocity profiles over time of all four wheel speed sensors are plotted. Similar to the previous two scenarios, the plots do not show any significant offsets. Even minor outliers are hardly visible.

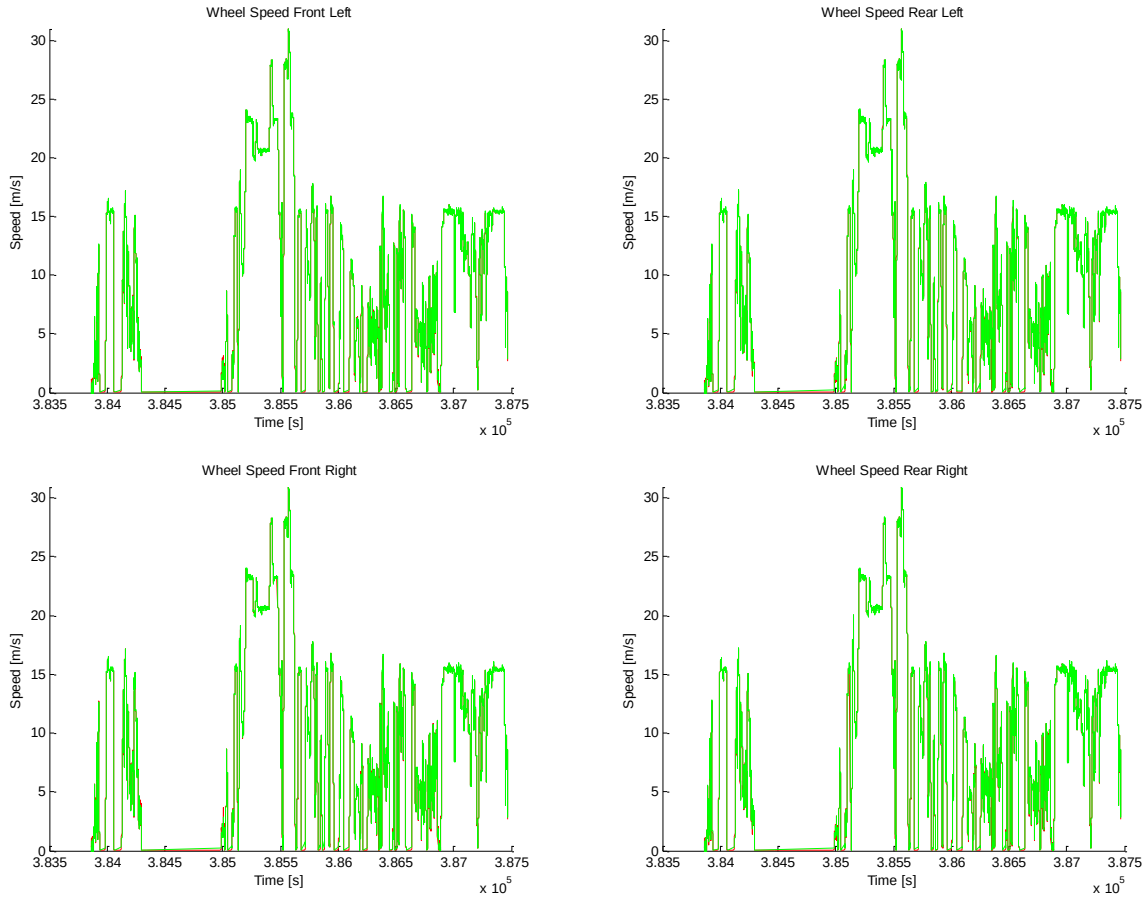

Abb. 41: Plots of real (green) and simulated (red) wheel speeds

The histogram plots showing the difference between simulated and real wheel speed sensor measurements are presented in Abb. 42. Outliers with an offset larger than 1 m/s are not present in the plot. The histograms show a zero-mean Gaussian behavior with a low variance.

Copyright © 2013, TEGA Konsortium. Alle Rechte vorbehalten.

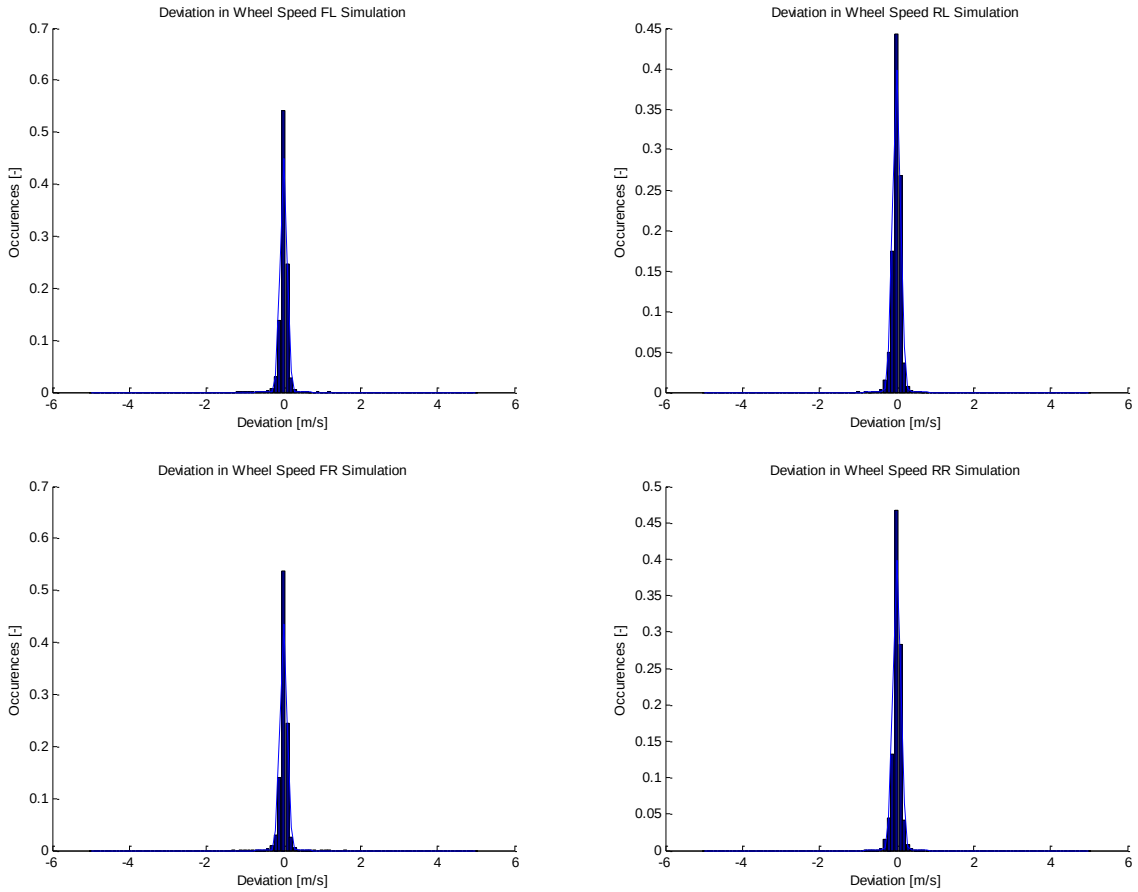

Abb. 42: Histogram plots of the deviation in the wheel speeds

Tab. 6 shows the corresponding mean values and standard deviations of the offset between measurements and simulation. In accordance with the previous two scenarios the mean offsets are in the order of 10^{-3} m/s. The standard deviation values are slightly larger than in the pure highway scenario but smaller compared to the combined highway/urban/rural scenario in the order of 10^{-1} m/s. In agreement with the previous scenarios the conclusion of this evaluation is that a realistic simulation is granted from the implemented system.

Tab. 6 Mean values and standard deviation of the offsets between simulated and real wheel speeds

Wheel	***Mean Offset [m/s]***	***Standard Deviation [m/s]***
Front Left	0.0057	0.0885
Front Right	0.0034	0.0917

Copyright © 2013, TEGA Konsortium. Alle Rechte vorbehalten.

Rear Left	0.0013	0.1002
Rear Right	0.0098	0.0998

Concluding this section the accumulated probability plots of the deviation is presented in Abb. 43. In compliance with the previous scenarios the wheel speed sensors show a reasonable behavior. The offset of more than 90% of the simulated measurements is less than 0.2 m/s from the real-life measurement data.

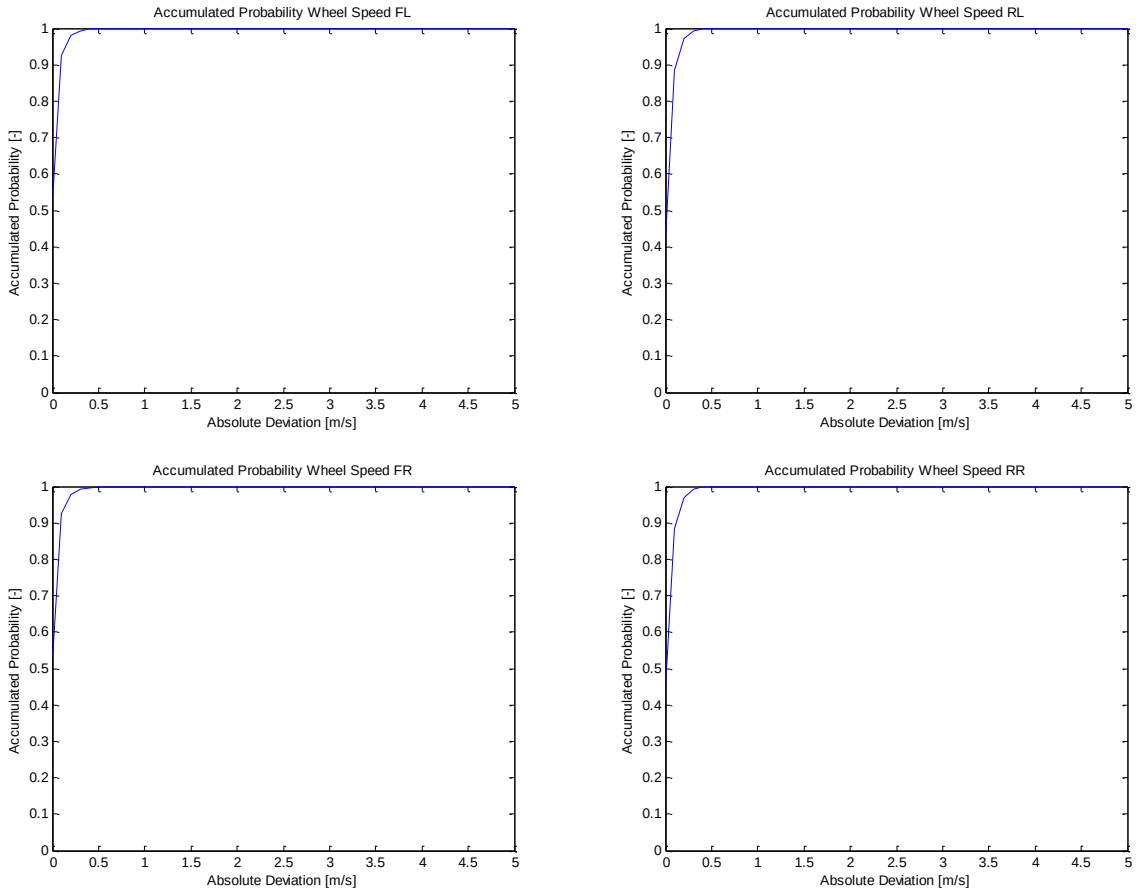

Abb. 43: Accumulated probability of the wheel speed deviation

Copyright © 2013, TEGA Konsortium. Alle Rechte vorbehalten.

B.5 Conclusions

This document presents the results of the TEGA AP 3500 “Experimentelle Validierung ‚Fahrzeugdynamik’”. In the first section, the evaluation strategy is presented. Based on the strategy, the experimental setup both for test drives and the laboratory are derived as it is feasible to compare real life measurement data with simulated vehicle data. A test vehicle is equipped with measurement equipment for allowing both capturing a reference trajectory and the sensor measurements. The laboratory setup then generates the simulated GNSS signal and the vehicle measurements derived from the reference trajectory.

The analysis of the gathered data is conducted in post process using an analysis tool written in Matlab. The recorded data from the reference system and the vehicle sensor data are preprocessed. Corresponding to the vehicle’s position and velocity a second data set containing the sensor measurements is recorded and processed. The evaluation process then consists of the comparison of the simulated and real life vehicle sensor measurements at every time stamp both values exist. The differences between them are evaluated, e.g. concerning scattering or systematic offsets.

Several test drives have been evaluated in the region of Braunschweig. Different environments such as rural roads and highways have been chosen for evaluation. The evaluation of the sensor data in all scenarios shows positive results. It can be observed, that the simulated and the real measurement values are virtually congruent. No significant outliers are visible in the scenarios. Hardly any measurements with an offset larger than 1 m/s are present. A distinct zero-mean Gaussian distribution occurs with a small variance. The average offsets are in the order of 10^{-3} m/s. The standard deviation values are $10^{-2}…10^{-1}$ m/s. It can be concluded that a realistic simulation is granted by the implemented system.

Copyright © 2013, TEGA Konsortium. Alle Rechte vorbehalten.

C Matlab-Skripte

C.1 Trajectory_Generation.m

```
%% Skript zur Trajektorienaufarbeitung

clc;
clear all;
close all;

%% Definitionen

smoothing_width = 40;
do_smoothing = false;

%% Konstanten

A_WGS = 6378137.0;
e_WGS = 8.1819190842622e-2;

%% Vehicle Properties

l = 2.705;          % Radstand
epsilon = 0.775;    % halbe Spurweite

%% Daten einlesen

read_data_generated;

Euler_Angle = zeros(length(ECEF_Position(:,1)),3);
v_abs = zeros(length(ECEF_Position(:,1)),1);
v_HL = zeros(length(ECEF_Position(:,1))-1,1);
v_HR = zeros(length(ECEF_Position(:,1))-1,1);
v_VL = zeros(length(ECEF_Position(:,1))-1,1);
v_VR = zeros(length(ECEF_Position(:,1))-1,1);
delta = zeros(length(ECEF_Position(:,1))-1,1);
delta_L = zeros(length(ECEF_Position(:,1))-1,1);
delta_R = zeros(length(ECEF_Position(:,1))-1,1);

radius1a = zeros(length(ECEF_Position(:,1))-2,1);
radius1b = zeros(length(ECEF_Position(:,1))-2,1);
radius2 = zeros(length(ECEF_Position(:,1))-1,1);
kappa1a = zeros(length(ECEF_Position(:,1))-2,1);
kappa1b = zeros(length(ECEF_Position(:,1))-2,1);
kappa2 = zeros(length(ECEF_Position(:,1))-1,1);

ECEF_Position_delta = zeros(length(ECEF_Position(:,1)), 3);
NED_Position = zeros(length(ECEF_Position(:,1)), 3);
v_NED_dot = zeros(length(ECEF_Position(:,1))-1, 3);
ECEF_Position_dot = zeros(length(ECEF_Position(:,1))-1, 3);
ECEF_Position_dotdot = zeros(length(ECEF_Position(:,1))-2, 3);

Psi_dot1a = zeros(length(ECEF_Position(:,1))-2,1);
```

Copyright © 2013, TEGA Konsortium. Alle Rechte vorbehalten.

```
Psi_dot1b = zeros(length(ECEF_Position(:,1))-2,1);
Psi_dot2 = zeros(length(ECEF_Position(:,1))-1,1);

if(do_smoothing)
    ECEF_Position_smooth = zeros(length(ECEF_Position(:,1)),3);
    ECEF_Position_dot_smooth = zeros(length(ECEF_Position(:,1))-1, 3);
    v_NED_smooth = zeros(length(ECEF_Position(:,1)), 3);
    v_NED_dot_smooth = zeros(length(ECEF_Position(:,1))-1, 3);
    ECEF_Position_dotdot_smooth = zeros(length(ECEF_Position(:,1))-2, 3);
end

%% Aufbereitung der Trajektorie
ECEF_Position_mean = mean(ECEF_Position);
[WGS_Position_mean(1), WGS_Position_mean(2), WGS_Position_mean(3)] =
cart2geo(ECEF_Position_mean(1), ECEF_Position_mean(2),
ECEF_Position_mean(3), 5);

slat = sind(WGS_Position_mean(1));
clat = cosd(WGS_Position_mean(1));
slon = sind(WGS_Position_mean(2));
clon = cosd(WGS_Position_mean(2));

M_NG = [-slat*clon  -slat*slon      clat;
        -slon        clon           0;
        -clat*clon  -clat*slon     -slat];

for i = 1:length(ECEF_Position(:,1))
    ECEF_Position_delta(i,:) = ECEF_Position(i,:) - ECEF_Position_mean;
    NED_Position(i,:) = M_NG *  ECEF_Position_delta(i,:)';
end

clear clat slat clon slon NED_Pos M_NG

if(do_smoothing)
    ECEF_Position_smooth(:,1) = smooth(ECEF_Position(:,1),
smoothing_parameter, 'rloess');
    disp('Smoothing Done x');
    ECEF_Position_smooth(:,2) = smooth(ECEF_Position(:,2),
smoothing_parameter, 'rloess');
    disp('Smoothing Done y');
    ECEF_Position_smooth(:,3) = smooth(ECEF_Position(:,3),
smoothing_parameter, 'rloess');
    disp('Smoothing Done z');

    v_NED_smooth(:,1) = smooth(v_NED(:,1), smoothing_parameter, 'rloess');
    disp('Smoothing Done v_N');
    v_NED_smooth(:,2) = smooth(v_NED(:,2), smoothing_parameter, 'rloess');
    disp('Smoothing Done v_E');
    v_NED_smooth(:,3) = smooth(v_NED(:,3), smoothing_parameter, 'rloess');
    disp('Smoothing Done v_D');
end

if(do_smoothing)
    for i = 1:length(ECEF_Position(:,1))
```

Copyright © 2013, TEGA Konsortium. Alle Rechte vorbehalten.

```
        %% Eulerwinkel aus v_NED_smooth

        Euler_Angle(i,1) = 0;
        Euler_Angle(i,2) = atan2(-v_NED_smooth(i,3),
sqrt(v_NED_smooth(i,1)^2 + v_NED_smooth(i,2)^2));
        Euler_Angle(i,3) = atan2(v_NED_smooth(i,2), v_NED_smooth(i,1));

    end

    for i = 1:(length(ECEF_Position(:,1))-1)
        ECEF_Position_dot(i,1) = ECEF_Position_smooth(i+1,1) -
ECEF_Position_smooth(i,1);
        ECEF_Position_dot(i,2) = ECEF_Position_smooth(i+1,2) -
ECEF_Position_smooth(i,2);
        ECEF_Position_dot(i,3) = ECEF_Position_smooth(i+1,3) -
ECEF_Position_smooth(i,3);

        v_NED_dot(i,1) = (v_NED_smooth(i+1,1) - v_NED(i,1))/(time(i+1) -
time(i));
        v_NED_dot(i,2) = (v_NED_smooth(i+1,2) - v_NED(i,2))/(time(i+1) -
time(i));
        v_NED_dot(i,3) = (v_NED_smooth(i+1,3) - v_NED(i,3))/(time(i+1) -
time(i));
    end
else
    for i = 1:length(ECEF_Position(:,1))

        %% Eulerwinkel aus v_NED

        Euler_Angle(i,1) = 0;
        Euler_Angle(i,2) = atan2(-v_NED(i,3), sqrt(v_NED(i,1)^2 +
v_NED(i,2)^2));
        Euler_Angle(i,3) = atan2(v_NED(i,2), v_NED(i,1));
    end

    for i = 1:(length(ECEF_Position(:,1))-1)
        ECEF_Position_dot(i,1) = ECEF_Position(i+1,1) - ECEF_Position(i,1);
        ECEF_Position_dot(i,2) = ECEF_Position(i+1,2) - ECEF_Position(i,2);
        ECEF_Position_dot(i,3) = ECEF_Position(i+1,3) - ECEF_Position(i,3);

        v_NED_dot(i,1) = (v_NED(i+1,1) - v_NED(i,1))/(time(i+1) - time(i));
        v_NED_dot(i,2) = (v_NED(i+1,2) - v_NED(i,2))/(time(i+1) - time(i));
        v_NED_dot(i,3) = (v_NED(i+1,3) - v_NED(i,3))/(time(i+1) - time(i));
    end
end


if(do_smoothing)
    ECEF_Position_dot_smooth(:,1) = smooth(ECEF_Position_dot(:,1),
smoothing_parameter, 'rloess');
    disp('Smoothing Done x_dot');
    ECEF_Position_dot_smooth(:,2) = smooth(ECEF_Position_dot(:,2),
smoothing_parameter, 'rloess');
```

Copyright © 2013, TEGA Konsortium. Alle Rechte vorbehalten.

```
    disp('Smoothing Done y_dot');
    ECEF_Position_dot_smooth(:,3) = smooth(ECEF_Position_dot(:,3),
smoothing_parameter, 'rloess');
    disp('Smoothing Done z_dot');


    for i = 1:(length(ECEF_Position_dot(:,1))-1)
        ECEF_Position_dotdot(i,1) = ECEF_Position_dot_smooth(i+1,1) -
ECEF_Position_dot_smooth(i,1);
        ECEF_Position_dotdot(i,2) = ECEF_Position_dot_smooth(i+1,2) -
ECEF_Position_dot_smooth(i,2);
        ECEF_Position_dotdot(i,3) = ECEF_Position_dot_smooth(i+1,3) -
ECEF_Position_dot_smooth(i,3);
    end

else

    for i = 1:(length(ECEF_Position_dot(:,1))-1)
        ECEF_Position_dotdot(i,1) = ECEF_Position_dot(i+1,1) -
ECEF_Position_dot(i,1);
        ECEF_Position_dotdot(i,2) = ECEF_Position_dot(i+1,2) -
ECEF_Position_dot(i,2);
        ECEF_Position_dotdot(i,3) = ECEF_Position_dot(i+1,3) -
ECEF_Position_dot(i,3);
    end

end

if(do_smoothing)
    ECEF_Position_dotdot_smooth(:,1) = smooth(ECEF_Position_dotdot(:,1),
smoothing_parameter, 'rloess');
    disp('Smoothing Done x_dotdot');
    ECEF_Position_dotdot_smooth(:,2) = smooth(ECEF_Position_dotdot(:,2),
smoothing_parameter, 'rloess');
    disp('Smoothing Done y_dotdot');
    ECEF_Position_dotdot_smooth(:,3) = smooth(ECEF_Position_dotdot(:,3),
smoothing_parameter, 'rloess');
    disp('Smoothing Done z_dotdot');

    ECEF_Position_dotdot = ECEF_Position_dotdot_smooth;
end

clear i;

%% Berechnung von Radius und Gierrate Option 1ab

M_NG = zeros(3,3);
M_BN = zeros(3,3);
M_BG = zeros(3,3);

for i = 1:(length(ECEF_Position_dot(:,1))-1)

    clat = cos(WGS_Position(i+1,1));
    slat = sin(WGS_Position(i+1,1));
```

Copyright © 2013, TEGA Konsortium. Alle Rechte vorbehalten.

```
    clon = cos(WGS_Position(i+1,2));
    slon = sin(WGS_Position(i+1,2));

    croll = cos(Euler_Angle(i+1,1));
    sroll = sin(Euler_Angle(i+1,1));
    cpitch = cos(Euler_Angle(i+1,2));
    spitch = sin(Euler_Angle(i+1,2));
    cyaw = cos(Euler_Angle(i+1,3));
    syaw = sin(Euler_Angle(i+1,3));

    M_NG = [-slat*clon  -slat*slon      clat;
            -slon        clon           0;
            -clat*clon  -clat*slon     -slat];

    M_BN = [      cpitch*cyaw                      cpitch*syaw
-spitch;
            sroll*spitch*cyaw - croll*syaw  sroll*spitch*syaw + croll*cyaw
sroll*cpitch;
            croll*spitch*cyaw + sroll*syaw  croll*spitch*syaw - sroll*cyaw
croll*cpitch];

    M_BG = M_BN * M_NG;

    x_dot = M_BG * (ECEF_Position_dot(i,:)' + ECEF_Position_dot(i+1,:)')/2;
    x_dotdot = M_BG * ECEF_Position_dotdot(i,:)';

    v = M_BN * v_NED(i,:)';
    v_dot = M_BN * v_NED_dot(i,:)';

    kappa1a(i) = (x_dot(1)*x_dotdot(2) - x_dot(2)*x_dotdot(1)) /
sqrt((x_dot(1)^2 + x_dot(2)^2)^3);
    radius1a(i) = 1/kappa1a(i);
    Psi_dot1a(i) = norm(v_ECEF(i,:)) * kappa1a(i) / cos(Euler_Angle(i,2));

    kappa1b(i) = (v(1)*v_dot(2) - v(2)*v_dot(1)) / sqrt((v(1)^2 +
v(2)^2)^3);
    radius1b(i) = 1/kappa1b(i);
    Psi_dot1b(i) = norm(v_ECEF(i,:)) * kappa1b(i) / cos(Euler_Angle(i,2));
end

clear clat slat clon slon croll sroll cpitch spitch cyaw syaw i M_NG M_BN
M_BG v v_dot x_dot x_dotdot;

mean_radius1a = mean(radius1a);
std_radius1a = std(radius1a);

mean_radius1b = mean(radius1b);
std_radius1b = std(radius1b);


%% Berechnung von Radius und Gierrate Option 2

for i = 1:length(ECEF_Position_dot(:,1))
```

Copyright © 2013, TEGA Konsortium. Alle Rechte vorbehalten.

```
    Psi_dot2(i) = (Euler_Angle(i+1,3) - Euler_Angle(i,3))/(time(i+1) -
time(i));
    kappa2(i) = Psi_dot2(i) * cos(Euler_Angle(i,2)) / norm(v_ECEF(i,:));
    radius2(i) = 1/kappa2(i);
end

clear i;

mean_radius2 = mean(radius2);
std_radius2 = std(radius2);

%% Berechnung von Geschwindigkeit, Radgeschwindigkeiten und Lenkwinkeln

for i = 1:length(ECEF_Position(:,1))

    v_abs(i) = norm(v_ECEF(i,:));

end

for i = 1:(length(ECEF_Position(:,1))-1)

    v_HL(i) = v_abs(i) * (1 + epsilon * kappa2(i));
    v_HR(i) = v_abs(i) * (1 - epsilon * kappa2(i));
    v_VL(i) = v_abs(i) * sqrt(1 + 2 * epsilon * kappa2(i) + (kappa2(i))^2 *
(l^2 + epsilon^2));
    v_VR(i) = v_abs(i) * sqrt(1 - 2 * epsilon * kappa2(i) + (kappa2(i))^2 *
(l^2 + epsilon^2));

    delta(i) = atand(l * kappa2(i));
    delta_L(i) = atand((l * tand(delta(i)))/(l + epsilon *
tand(delta(i))));
    delta_R(i) = atand((l * tand(delta(i)))/(l - epsilon *
tand(delta(i))));

end

clear i;

%% Plots erzeugen

figure;
plot(NED_Position(:,1), NED_Position(:,2));
daspect([1 1 1]);
axis([-250 250 -250 250]);
xlabel('NED Position x [m]');
ylabel('NED Position y [m]');
title('Trajectory in NED coordinates (x-y-plane)');

figure;
subplot(1,2,1);
plot(time, Euler_Angle(:,2)*180/pi);
xlabel('Time [s]');
ylabel('Pitch Angle [°]');
title('Pitch Angle');
```

Copyright © 2013, TEGA Konsortium. Alle Rechte vorbehalten.

```
% figure;
subplot(1,2,2);
plot(time, Euler_Angle(:,3)*180/pi);
xlabel('Time [s]');
ylabel('Heading [°]');
title('Heading');

figure;
plot(time(1:(length(time)-2)), radius1a);
xlabel('Time [s]');
ylabel('Radius [m]');
title('Trajectory Radius using Option 1a');

figure;
plot(time(1:(length(time)-2)), radius1b);
xlabel('Time [s]');
ylabel('Radius [m]');
%ylim([-200.15 -199.85]);
title('Trajectory Radius using Option 1b');

figure;
plot(time(1:(length(time)-1)), radius2);
xlabel('Time [s]');
ylabel('Radius [m]');
%ylim([-200.15 -199.85]);
title('Trajectory Radius using Option 2');

figure;
hold on;
plot(time(1:length(time)), v_abs, 'b');
plot(time(1:(length(time)-1)), v_HL, 'm');
plot(time(1:(length(time)-1)), v_HR, 'c');
plot(time(1:(length(time)-1)), v_VL, 'r');
plot(time(1:(length(time)-1)), v_VR, 'g');
legend('v', 'v_{HL}', 'v_{HR}', 'v_{VL}', 'v_{VR}');
xlabel('Time [s]');
ylabel('Wheel Speeds [m/s]');
title('Wheel Speeds');
hold off;

figure;
hold on;
plot(time(1:(length(time)-1)), delta, 'b');
plot(time(1:(length(time)-1)), delta_L, 'r');
plot(time(1:(length(time)-1)), delta_R, 'g');
legend('\delta', '\delta_L', '\delta_R');
xlabel('Time [s]');
ylabel('Steering Angle [°]');
title('Steering Angle');
hold off;
```

Copyright © 2013, TEGA Konsortium. Alle Rechte vorbehalten.

C.2 read_data_generated.m

```
path = 'H:\GNSS\TU3000\src\Matlab\TEGA\Datensatz TEGA\';
filename = 'NavXCircleGlobal20mps.txt';

file = strcat(path, filename);

data = dlmread(file, ' ', 1,0);

clear path filename file;

smoothing_parameter = smoothing_width / length(data(:,1));

time = zeros(length(data(:,1)), 1);
WGS_Position = zeros(length(data(:,1)), 3);
ECEF_Position = zeros(length(data(:,1)), 3);
v_NED = zeros(length(data(:,1)), 3);
v_ECEF = zeros(length(data(:,1)), 3);

%% Datenumrechnung

for i = 1:length(data(:,1))

    time(i) = data(i,1);

    ECEF_Position (i,1) = data(i,2);
    ECEF_Position (i,2) = data(i,3);
    ECEF_Position (i,3) = data(i,4);

    %%v_ECEF

    v_ECEF(i,1) = data(i,5);
    v_ECEF(i,2) = data(i,6);
    v_ECEF(i,3) = data(i,7);

    %% WGS Pos berechnen

    [lat, lon, alt] = cart2geo(ECEF_Position (i,1), ECEF_Position (i,2),
ECEF_Position (i,3), 5);

    WGS_Position(i,1) = lat * pi/180;
    WGS_Position(i,2) = lon * pi/180;
    WGS_Position(i,3) = alt;

    %% v_NED bilden

    clat = cos(WGS_Position(i,1));
    slat = sin(WGS_Position(i,1));
    clon = cos(WGS_Position(i,2));
    slon = sin(WGS_Position(i,2));

    M_NG = [-slat*clon -slon -clat*clon ;
```

Copyright © 2013, TEGA Konsortium. Alle Rechte vorbehalten.

```
            -slat*slon  clon -clat*slon ;
            clat        0    -slat      ];

    v = M_NG' * [v_ECEF(i,1) v_ECEF(i,2) v_ECEF(i,3)]';

    v_NED(i,1) = v(1);
    v_NED(i,2) = v(2);
    v_NED(i,3) = v(3);


    %% Eulerwinkel
end

clear x N data i clat clon slat slon lat lon alt;
```

Copyright © 2013, TEGA Konsortium. Alle Rechte vorbehalten.